A stress-dependent TRIM28–ALKBH2 feedback loop modulates chemotherapy response

Zhiming Sun, Yunfang Deng, Yue Liu, Zhaohui Liu, Jiabing Li, Lihui Wu, Liyuan Zeng, Xiaorong Feng, Lin Miao, Ying Sheng, Bei Chen, Yuming He, Ye Liu & Yu Zhao*

The National & Local Joint Engineering Laboratory of Animal Peptide Drug Development, College of Life Sciences, Hunan Normal University, Changsha, Hunan, 410081, China

* Corresponding author: Yu Zhao (smile_zhao@hotmail.com)

Running title: TRIM28–ALKBH2 modulates chemoresistance

Keywords: TRIM28, ALKBH2, MAGEA6, Ubiquitination, Chemoresistance

ABSTRACT

Chemoresistance to DNA-damaging agents, including platinum and alkylating compounds, remains a major limitation in the treatment of non-small cell lung cancer (NSCLC), often correlated with upregulated DNA repair. Here, we define a reciprocal regulatory loop between the E3 ligase TRIM28 and the alkylation repair enzyme ALKBH2. TRIM28 directly binds ALKBH2 and mediates its K48-linked polyubiquitination and proteasomal degradation, whereas ALKBH2 reciprocally enhances TRIM28 transcription, establishing a homeostatic equilibrium. Upon alkylation stress, acute MMS exposure enhances assembly of the TRIM28–ALKBH2 complex, a process facilitated by MAGEA6, and promotes ALKBH2 degradation. In contrast, prolonged MMS exposure induces K48-linked ubiquitination and degradation of TRIM28, leading to ALKBH2 stabilization and transcriptional upregulation. Clinically, ALKBH2 is elevated in lung adenocarcinoma and correlates with poor prognosis; notably, high TRIM28 expression specifically correlates with poor survival in patients receiving chemotherapy. Moreover, the combination of MMS and cisplatin enhances DNA damage and attenuates ALKBH2-mediated chemoresistance. Collectively, these findings define a stress-responsive TRIM28–ALKBH2 feedback loop that modulates alkylation responses and shapes chemotherapy sensitivity.

Introduction

Cells are continuously challenged by endogenous metabolites and environmental or therapeutic alkylating agents that generate cytotoxic and mutagenic DNA adducts, posing a constant threat to genome integrity (Fu, Calvo et al., 2012, Zhao, Majid et al., 2015). To counteract this, cells utilize three principal repair strategies: base excision repair (BER), direct reversal by O^6-methylguanine-DNA methyltransferase (MGMT), and oxidative demethylation catalyzed by the AlkB family of Fe(II)/α-ketoglutarate–dependent dioxygenases (Drabløs, Feyzi et al., 2004, Li, Feng et al., 2025, Soll, Sobol et al., 2017). These dioxygenases specifically target N-linked methyl lesions (e.g., 1-meA and 3-meC) through a coupled oxidative reaction, restoring the unmodified base without requiring nucleotide excision (Leiros, Nabong et al., 2007, Trewick, Henshaw et al., 2002). This direct reversal mechanism provides an evolutionarily conserved and critical defense against alkylation toxicity (Yi & He, 2013). In mammals, the AlkB homologues complement BER and MGMT to resolve specific lesions that escape other repair systems, thereby ensuring efficient genomic maintenance under both physiological and pathological stress (Xu & Bochtler, 2020).

Among the nine mammalian AlkB homologues, the demethylase ALKBH2 serves as the principal enzyme for repairing methylated bases in duplex DNA, a function essential for preventing alkylation-induced mutagenesis (Duncan, Trewick et al., 2002). Loss or functional impairment of ALKBH2 results in hypersensitivity to alkylating agents and the accumulation of cytotoxic base lesions, underscoring its nonredundant role in resolving adducts that escape other repair pathways (Li, Huang et al., 2016, Ringvoll, Nordstrand et al., 2006, Wang, Wu et al., 2015). Clinically, ALKBH2 is frequently upregulated in human cancers, particularly non–small cell lung cancer (NSCLC), where elevated expression correlates with increased repair capacity and chemoresistance (Johannessen, Prestegarden et al., 2013, Wang et al., 2015, Wu, Yan et al., 2021, Wu, Xu et al., 2011, Xu, Zhang et al., 2022). Given that alkylating chemotherapeutics (e.g., temozolomide) and environmental insults (e.g., cigarette smoke) generate similar methylated base lesions (Fu et al., 2012, Hegi, Diserens et al., 2005, Li, Zeng et al., 2024), the dynamic regulation of ALKBH2 constitutes a key determinant of tumor survival under sustained alkylation stress

(Johannessen et al., 2013, Wilson, Beharry et al., 2018). However, the specific post-translational mechanisms governing ALKBH2 protein stability and turnover remain poorly understood.

While the expression of AlkB family dioxygenases is modulated by diverse transcriptional and epigenetic programs (Chen, Zhou et al., 2025, Feng, Xu et al., 2022, Johannessen et al., 2013, Song, Feng et al., 2019, Wada, Naito et al., 2024), these enzymes are tightly controlled by dynamic ubiquitin-dependent regulation to ensure rapid proteostatic control. Extensive research has delineated the E3 ligase networks for other AlkB homologues, particularly FTO and ALKBH5. For instance, FTO turnover is regulated by multiple context-specific E3 ligases, including TRIM17, DTX2, MIB1, and RNF144A (Cui, Wei et al., 2024, Dai, Tian et al., 2024, Han, Tong et al., 2024, Liu, Zheng et al., 2025), while its degradation by TRIM21 is specifically primed by O-GlcNAcylation (Zhang, Liu et al., 2025). Similarly, ALKBH5 stability is controlled by the E3 ligase RNF180, or via PRMT5-mediated methylation, which primes it for recognition and ubiquitination by TRIM28 (Meng, Liu et al., 2025, Wang, Liu et al., 2024). Conversely, these degradative pathways are counterbalanced by a deubiquitinase (DUB) network, including USP7, USP14, USP18, and USP36. This regulation orchestrates dioxygenase homeostasis by stabilizing the demethylases FTO and ALKBH5 in a highly substrate-specific manner. For example, FTO is stabilized by USP7 (Lin, Zhou et al., 2023) and USP18 (Song, Yi et al., 2024), while USP14 (Zhou, Xia et al., 2025) and USP36 (Chang, Xie et al., 2023) stabilize ALKBH5. Our own previous work further extended this principle by identifying OTUD4 as a scaffolding DUB that stabilizes the demethylase ALKBH3 (Zhao et al., 2015). In stark contrast to these well-characterized homologues, the specific E3 ligase controlling ALKBH2 protein stability remains unidentified. However, a vital clue emerges from the ALKBH2-containing ASCC complex: its active recruitment of TRIM28 upon alkylation stress (MMS) (Brickner, Soll et al., 2017), thereby functionally positioning this E3 ligase within the alkylation repair machinery.

The tripartite motif (TRIM) family of RING-type E3 ligases, including TRIM24, TRIM28, and TRIM33, orchestrates ubiquitin signaling to couple chromatin remodeling with stress responses (Gu, Chen et al., 2023, Hatakeyama, 2011). As a key member of this subgroup, TRIM28

(KAP1), leverages its N-terminal RING domain and C-terminal PHD–BRD module to enforce KRAB-ZNF-dependent transcriptional silencing and maintain genomic stability (Czerwińska, Mazurek et al., 2017, Randolph, Hyder et al., 2022). While TRIM28 functions as a master corepressor and E3 ligase, its own functional state and availability are governed by a complex regulatory hierarchy. Classically, in response to DNA double-strand breaks (DSBs), TRIM28 undergoes rapid ATM/ATR-mediated phosphorylation at Ser824, a modification essential for relaxing heterochromatin to facilitate repair factor access (Goodarzi, Kurka et al., 2011, Lee, Goodarzi et al., 2012, Yalçin, Lam et al., 2024). Beyond these acute post-translational modifications, TRIM28 expression is tightly regulated at the transcriptional level by nuclear receptors such as NR3C2 (Li, Xie et al., 2025) and post-transcriptionally via NSUN2-mediated RNA methylation (m^5C) (Wang, Mierxiati et al., 2025) as well as stabilization by the lncRNA PITAR (Jana, Mondal et al., 2024). Furthermore, under stress conditions, TRIM28 protein abundance is dynamically regulated via the ubiquitin-proteasome system; specifically, its turnover is governed by the E3 ligase RNF4 during genotoxic stress and March5 under metabolic stress (Chen, Pang et al., 2025, Kuo, Li et al., 2014). Additionally, the substrate specificity of TRIM28 is often reprogrammed by melanoma-associated antigen (MAGE) proteins (Doyle, Gao et al., 2010, Kim, Lee et al., 2009, Xiao, Suh et al., 2014), such as MAGEA6, which act as substrate adaptors (Doyle et al., 2010, Li, Krone et al., 2024). However, the mechanistic interplay between TRIM28 and the alkylation repair machinery—particularly whether reciprocal feedback circuits coordinate their stability and expression under stress—remains largely unexplored.

In this study, TRIM28, together with the adaptor MAGEA6, is defined as the E3 ligase complex that regulates ALKBH2 stability through K48-linked polyubiquitination and proteasomal degradation under basal conditions. ALKBH2, in turn, enhances TRIM28 transcription, forming a homeostatic feedback loop that links E3 ligase activity to ALKBH2 turnover. Acute MMS exposure enhances assembly of the TRIM28–ALKBH2 complex and promotes ALKBH2 degradation, whereas prolonged MMS exposure induces K48-linked ubiquitination and degradation of TRIM28, resulting in ALKBH2 stabilization and transcriptional induction.

113 Together, these mechanisms reveal a stress-responsive TRIM28–MAGEA6–ALKBH2 feedback
114 loop that coordinates repair capacity with the dynamics of stress exposure and provides a
115 mechanistic basis for variations in chemotherapy response.

Results

TRIM28 directly binds ALKBH2

To identify proteins associated with TRIM28, we performed tandem affinity purification in H1299 non–small cell lung cancer (NSCLC) cells, followed by silver staining and LC–MS/MS. This analysis identified ALKBH2 as a putative interactor (Fig. 1A; Appendix Fig. S1A; Appendix Table S1). Co-immunoprecipitation (co-IP) in HEK293T cells co-expressing HA-tagged ALKBH2 and Flag-tagged TRIM28 confirmed this association, whereas the related paralog TRIM24 did not show detectable binding (Fig. 1B). Reciprocal co-IP using HA-ALKBH2 further validated the interaction (Fig. 1C). Domain mapping using TRIM28 truncation mutants demonstrated that the BCC region (B-box + coiled-coil; residues 141–400) was required for ALKBH2 binding (Fig. 1D, E). Endogenous co-IP in H1299 cells confirmed recovery of native ALKBH2 by the anti-TRIM28 antibody (Fig. 1F), and immunofluorescence analysis revealed strong nuclear co-localization of TRIM28 and ALKBH2 (Fig. 1G).

In vitro MBP pull-down assays using purified recombinant proteins demonstrated that TRIM28 directly binds ALKBH2 (Fig. 1H). Specificity profiling revealed a preferential interaction with ALKBH2 compared with the related demethylase ALKBH3 (Fig. 1I) or the direct-reversal repair enzyme MGMT (Appendix Fig. S1B). Protein–protein docking predicted a TRIM28–ALKBH2 interface overlapping the nucleic-acid-binding surface of ALKBH2, centered on the Finger (hairpin) motif and the flexible Long-loop (Yang, Yi et al., 2008), which are present in ALKBH2 but absent in ALKBH3 (Fig. 1J). Consistent with this model, single-stranded DNA (ssDNA) competitively reduced TRIM28–ALKBH2 binding in a dose-dependent manner (Fig. 1K), a strategy commonly used to probe DNA-occupied states of repair enzymes (Gu, Deng et al., 2013, Le, Ma et al., 2020). Collectively, these data reveal a direct and selective interaction between TRIM28 and ALKBH2 mediated by the TRIM28 BCC domain and indicate that DNA binding to ALKBH2 can competitively modulate this interaction.

142 **A reciprocal regulatory loop between TRIM28 and ALKBH2 governs the stability and**
143 **ubiquitination of ALKBH2**

144 To determine whether ALKBH2 undergoes ubiquitin-dependent modification, we performed
145 denaturing immunoprecipitation (IP) of Flag-ALKBH2 from HEK293T cells co-transfected with
146 HA-ubiquitin. A high-molecular-weight smear corresponding to polyubiquitinated ALKBH2 was
147 detected, and this signal markedly increased after proteasome inhibition with MG132 (Fig. 2A).
148 Expression of a K48-only ubiquitin mutant further enhanced ALKBH2 ubiquitination, whereas the
149 K48R mutant almost completely abolished it (Fig. 2B), indicating that ALKBH2 is predominantly
150 modified by K48-linked polyubiquitin chains. Consistently, Halo-TUBE pull-down enriched K48-
151 linked polyubiquitinated ALKBH2, confirming endogenous K48-linked ubiquitination (Fig. 2C).

152 We next examined whether TRIM28 mediates this modification. Overexpression of wild-type
153 (WT) TRIM28 increased K48-linked ubiquitination of ALKBH2 (Fig. 2D), whereas the RING-
154 inactive C65/68A mutant—previously shown to abolish TRIM28 E3 ligase activity (Doyle et al.,
155 2010)—failed to promote this modification (Fig. 2F). TRIM28 depletion using two independent
156 shRNAs markedly reduced ALKBH2 ubiquitination (Appendix Fig. S2A). Re-expression of
157 shRNA-resistant WT TRIM28 in TRIM28-knockdown cells restored ALKBH2 ubiquitination (Fig.
158 2E). These results demonstrate that TRIM28 E3 ligase activity is required for efficient K48-linked
159 ubiquitination of ALKBH2.

160 We then assessed how this modification affects ALKBH2 protein stability. TRIM28
161 knockdown in H1299 and A549 cells increased ALKBH2 protein levels without altering its mRNA
162 expression (Fig. 2G, H), and similar results were obtained upon CRISPR/Cas9-mediated TRIM28
163 depletion (Appendix Fig. S2B). Cycloheximide (CHX) chase assays revealed that TRIM28
164 knockdown extended ALKBH2 half-life, whereas enforced TRIM28 expression shortened it in a
165 RING-dependent manner (Appendix Fig. S2C, D). Increasing TRIM28 expression produced a
166 dose-dependent decrease in ALKBH2 protein abundance in both H1299 and HEK293T cells (Fig.
167 2I). These data indicate that TRIM28 limits ALKBH2 levels through proteasome-mediated
168 degradation rather than altered localization (Appendix Fig. S2E).

169 To determine whether ALKBH2 in turn regulates its E3 ligase, we depleted ALKBH2 in
170 H1299 cells using two independent shRNAs. TRIM28 protein levels were reduced following
171 ALKBH2 knockdown (Fig. 2J), and re-expression of Flag-ALKBH2 restored TRIM28 (Fig. 2K).
172 Overexpression of ALKBH2 further increased TRIM28 mRNA as measured by qRT-PCR (Fig.
173 2L). Consistent with this regulatory link, TCGA lung adenocarcinoma data revealed a positive
174 correlation between ALKBH2 and TRIM28 transcripts (Appendix Fig. S2F). Collectively, these
175 results define a reciprocal regulatory loop in which TRIM28 acts as an E3 ligase promoting K48-
176 linked ubiquitination and proteasomal degradation of ALKBH2, while ALKBH2 enhances
177 TRIM28 expression at the transcriptional level.
178

179 **MAGEA6 scaffolds the TRIM28–ALKBH2 E3 ligase complex, a function impaired by**
180 **cancer-associated variants**

181 Given that MAGE family proteins can associate with E3 ligases such as TRIM28 to modulate their
182 activity (Doyle et al., 2010, Feng, Gao et al., 2011), we examined the organization of the TRIM28–
183 ALKBH2 complex and the role of MAGEA6 in this process. Co-immunoprecipitation (co-IP) in
184 HEK293T cells revealed a previously unrecognized interaction between Myc-tagged MAGEA6
185 and the substrate ALKBH2 (Fig. 3A), which was further confirmed as direct by *in vitro* pull-down
186 assays using purified recombinant proteins (Fig. 3B).

187 We next investigated how MAGEA6 contributes to complex assembly. The MAGEA6–
188 ALKBH2 interaction was independent of TRIM28, as TRIM28 knockdown did not disrupt their
189 association (Fig. 3C), suggesting that MAGEA6 engages ALKBH2 before or independently of
190 TRIM28 recruitment. Overexpression of Myc-MAGEA6 enhanced TRIM28–ALKBH2 complex
191 formation in a dose-dependent manner (Fig. 3D; Fig. EV1A), whereas knockdown of endogenous
192 MAGEA3/6 attenuated this interaction (Fig. 3E). Because antibodies cannot distinguish between
193 the highly homologous MAGEA3 and MAGEA6 (96% sequence identity (Pineda, Ramanathan et
194 al., 2015)), they are referred to collectively as MAGEA3/6 throughout this study. The related

195 family member MAGEC2 exhibited a similar effect (Fig. EV1B), indicating a conserved
196 scaffolding function within this subfamily.

197 To determine the functional consequence of this scaffolded complex, we next assessed its
198 impact on ALKBH2 ubiquitination and stability. MAGEA6 knockdown reduced endogenous
199 ALKBH2 ubiquitination, and this reduction was rescued by re-expression of MAGEA6 (Fig.
200 EV1C). Conversely, MAGEA6 overexpression promoted K48-linked ubiquitination of ALKBH2,
201 but this effect was markedly diminished upon TRIM28 knockdown, confirming that it depends on
202 TRIM28 (Fig. 3F). Consistently, MAGEA6 accelerated ALKBH2 degradation in control cells,
203 whereas this effect was largely abolished in TRIM28-knockout H1299 cells (Fig. 3G).

204 Given that MAGEA6 mutations have been reported in multiple tumor types, including lung
205 cancer (Tsang, Wang et al., 2020), we examined whether cancer-associated variants affect this
206 regulatory axis. Sequencing of MAGEA6 cDNA from H1299 cells identified two variants, MutA
207 and MutB, harboring 12 and 20 amino acid substitutions, respectively (Fig. EV1D). Both mutants
208 were individually cloned and sequence-verified for functional testing. Co-IP assays revealed that
209 both MutA and MutB displayed weaker binding to ALKBH2, and MutB also showed reduced
210 association with TRIM28 (Fig. 3H). As a result, these variants exhibited impaired ability to
211 promote ALKBH2 ubiquitination and degradation compared with wild-type MAGEA6 (Fig. 3I;
212 Fig. EV1E).

213 To further delineate the molecular basis of this interaction, AlphaFold3 modeling predicted a
214 contact interface between MAGEA6 and TRIM28 (Fig. EV1F), encompassing residues D156 and
215 S157 within the MAGE homology domain. Notably, the S157 site is found in the MutB variant
216 and corresponds to tumor-associated mutations reported in COSMIC: S157 (MAGEA6, COSMIC
217 ID: 1715821, melanoma) and its homologous position in MAGEA3 (S157, COSMIC ID: 3559357,
218 detected in lung cancer, lymphoma, and melanoma). Functional assays showed that mutating these
219 residues (D156E/S157Y) markedly reduced TRIM28 binding and impaired MAGEA6-mediated
220 ALKBH2 degradation (Fig. 3J; Fig. EV1H). In contrast, a K211R substitution within the predicted
221 ALKBH2-binding surface had only a modest effect on their association (Fig. 3J). Collectively,

222 these findings define MAGEA6 as a scaffolding cofactor that directly associates with ALKBH2
223 and recruits TRIM28 to promote its ubiquitination and degradation. Cancer-associated variants
224 that disrupt the MAGEA6–TRIM28 interface compromise this regulatory function, potentially
225 contributing to defective DNA repair regulation in tumors.
226

227 **MMS drives a biphasic ALKBH2 response, from acute degradation to prolonged**
228 **accumulation**

229 **MMS acutely promotes ALKBH2 degradation**

230 To investigate how MMS regulates the TRIM28–ALKBH2 axis, we analyzed their interaction
231 dynamics in H1299 cells. Short-term MMS exposure (3–6 h) progressively enhanced the
232 TRIM28–ALKBH2 association in a time- and dose-dependent manner (Fig. 4A, B). While both
233 proteins remained predominantly nuclear (Fig. EV2A), MAGEA3/6 accumulated in the nucleus
234 upon MMS treatment (Fig. 4C), suggesting that MAGEA3/6 facilitates assembly of the TRIM28–
235 ALKBH2 complex during genotoxic stress. Consistent with this, MMS increased K48-linked
236 ubiquitination of ALKBH2 in a concentration-dependent manner (Fig. 4D). To exclude
237 transcriptional effects, we used H1299 cells stably expressing TAP-tagged ALKBH2. MMS
238 exposure accelerated ALKBH2 degradation, which was further enhanced by TRIM28
239 overexpression (Fig. 4E). Similarly, endogenous ALKBH2 exhibited reduced stability when cells
240 were co-treated with MMS and cycloheximide (CHX), compared with CHX alone (Fig. EV2B, C).
241 These data define an acute response phase in which MMS enhances TRIM28-dependent
242 ubiquitination and degradation of ALKBH2.

243 Because alkylating agents such as MMS and temozolomide (TMZ) are known to elevate
244 intracellular ROS levels (Bu, Qu et al., 2021, Lombard, Kohler et al., 2020, Zhao, Zheng et al.,
245 2017), we next examined whether redox balance modulates the TRIM28–ALKBH2 interaction. In
246 co-immunoprecipitation assays, H_2O_2 enhanced complex formation, whereas single-stranded
247 DNA (ssDNA), ascorbate (Vc), or EDTA weakened the interaction (Fig. 4F). Reduced glutathione
248 (GSH) attenuated TRIM28–ALKBH2 binding, while oxidized glutathione (GSSG) had little effect.
249 GSH also blunted the H_2O_2-induced enhancement (Fig. EV2D). Similarly, EDTA decreased basal

250 interaction and prevented H_2O_2-driven binding (Fig. 4G). In agreement, oxidative stress alone was
251 sufficient to trigger ubiquitination, as H_2O_2 increased K48-linked polyubiquitination of ALKBH2
252 in a dose-dependent manner (Fig. EV2E).

253 In contrast, the catalytically inactive ALKBH2(H171A/D173A) mutant (Lee, Jin et al., 2005,
254 Yang et al., 2008) failed to display the ssDNA-dependent reduction or H_2O_2-induced enhancement
255 of TRIM28 binding, suggesting that this redox control is coupled to the catalytic state of ALKBH2
256 (Fig. EV2F). Furthermore, the reducing agent Vc suppressed MMS-induced K48-linked
257 ubiquitination of ALKBH2 (Fig. 4H). Together, these results identify an acute MMS response
258 characterized by redox-sensitive, TRIM28-dependent ubiquitination leading to ALKBH2
259 degradation.

260 **Prolonged MMS exposure stabilizes ALKBH2**

261 In contrast to the early degradative phase, prolonged MMS exposure (≥8 h) led to recovery and
262 accumulation of ALKBH2 protein. MMS treatment increased ALKBH2 abundance in both H1299
263 and H460 cells, with variable induction levels between lines (Fig. 4I, J). The protein levels of
264 ALKBH3 and MGMT remained unchanged (Fig. 4I). Moreover, TRIM28 overexpression
265 attenuated MMS-induced ALKBH2 accumulation (Fig. 4K). These data indicate that prolonged
266 MMS treatment shifts ALKBH2 regulation from degradation to stabilization.

267 **Prolonged MMS exposure induces transcriptional upregulation of ALKBH2**

268 To determine whether ALKBH2 accumulation involves transcriptional activation, total RNA was
269 isolated from H1299 cells after MMS exposure for the indicated durations and analyzed by qRT–
270 PCR. A significant increase in ALKBH2 transcript abundance was observed at 12 h and sustained
271 at 24 h (Fig. 4L), consistent with the delayed protein induction. Collectively, these data define a
272 biphasic regulatory pattern of ALKBH2 under MMS exposure—an early, post-translational phase
273 marked by TRIM28-dependent ubiquitination and degradation, followed by a late, transcriptional
274 phase characterized by ALKBH2 stabilization and transcriptional upregulation.

275

276 **MMS promotes K48-linked ubiquitination and proteasomal degradation of TRIM28**
277 **facilitated by TRIM24 and MAGEA6**

278 To investigate how TRIM28 is regulated during alkylation stress, we examined its protein stability
279 and post-translational modification. MMS treatment caused a time- and dose-dependent decrease
280 in TRIM28 protein without affecting its mRNA (Fig. 5A–C), and this reduction was blocked by
281 the proteasome inhibitor MG132, indicating proteasome-dependent degradation. Prolonged low-
282 dose MMS exposure (100 μM, 24–72 h) led to progressive accumulation of ALKBH2, whereas
283 other repair proteins, including ALKBH3, MGMT, and MAGEA3/6, remained unchanged (Fig.
284 EV3A). Consistent with this relationship, pre-exposure to MMS for 12 h caused TRIM28 depletion,
285 elevated basal ALKBH2 levels, and delayed ALKBH2 turnover (Fig. EV3B, C), supporting the
286 notion that TRIM28 loss contributes to ALKBH2 stabilization during prolonged alkylation stress.
287 To define the underlying mechanism, we next analyzed TRIM28 ubiquitination. Denaturing
288 immunoprecipitation of tagged TRIM28 showed that MMS robustly induced its polyubiquitination
289 (Fig. 5D), which increased in a time-dependent manner in H1299 cells (Fig. 5E). Use of a K48-
290 only ubiquitin mutant confirmed that these modifications are mainly K48-linked, consistent with
291 proteasomal targeting (Fig. 5F). Endogenous analysis using K48-specific Halo-TUBE pulldown
292 verified MMS-induced ubiquitination under physiological conditions (Fig. 5G). In contrast, other
293 genotoxic agents—including TMZ, CDDP, and H_2O_2—failed to trigger either K48-linked
294 ubiquitination or TRIM28 degradation (Fig. 5H; Fig. EV3D–F). Notably, TMZ increased
295 ALKBH2 protein without altering TRIM28 levels (Fig. EV3D), whereas H_2O_2 decreased
296 ALKBH2 but not TRIM28, and CDDP had little effect on either (Fig. EV3E, F). These
297 observations indicate that TRIM28 degradation is a specific response to alkylation stress rather
298 than a general feature of DNA damage.
299 To test whether SUMOylation contributes to MMS-induced ubiquitination, we examined a
300 SUMO-acceptor-deficient TRIM28 mutant (K554/779/804R) (Ivanov, Peng et al., 2007). K48-
301 specific Halo-TUBE pulldown revealed markedly reduced ubiquitination in the triple-lysine
302 mutant compared with wild-type TRIM28 (Fig. 5I), suggesting that MMS-triggered ubiquitination
303 occurs at—or is influenced by—the same lysine cluster targeted for SUMOylation.

304 To identify upstream regulators, we next analyzed the TRIM28 interactome (Appendix Table
305 S2) and validated selected candidates. MMS increased TRIM28 association with the E3 ligase
306 TRIM24 and with the proteasome subunits PSMD4 and PSMB5 in a time-dependent manner (Fig.
307 5J). These interactions were diminished in the SUMO-acceptor mutant (Fig. EV3G). The scaffold
308 protein MAGEA6 enhanced formation of the TRIM28–TRIM24 complex; under MMS treatment,
309 co-expression of MAGEA6 further strengthened TRIM28 binding to TRIM24 and to
310 PSMD4/PSMB5, accompanied by increased K48-linked polyubiquitination (Fig. 5K). Reciprocal
311 co-immunoprecipitation using Flag-TRIM24 confirmed the MMS-inducible TRIM28–TRIM24
312 interaction and revealed that TRIM24 itself underwent K48-linked ubiquitination upon MMS
313 exposure (Fig. 5L). Overexpression of TRIM24 further amplified MMS-induced ubiquitination
314 and loss of endogenous TRIM28, as shown by Halo-TUBE pulldown and immunoblotting (Figs.
315 5M and EV3H, I). Collectively, these data demonstrate that MMS specifically promotes K48-
316 linked ubiquitination and proteasomal degradation of TRIM28 through a pathway coordinated by
317 MAGEA6, TRIM24, and SUMO-associated regulation. This stress-specific mechanism places
318 TRIM28 within a broader alkylation-responsive ubiquitin network distinct from other DNA-
319 damage responses.
320

321 **The TRIM28–ALKBH2 axis links clinical outcome with cellular responses to alkylation**
322 **stress**

323 To assess the clinical relevance of this pathway in lung adenocarcinoma (LUAD), we first
324 examined ALKBH family expression. Analysis of TCGA (mRNA) and CPTAC (proteomic)
325 datasets revealed significantly increased ALKBH2 and decreased ALKBH3, whereas MGMT
326 levels were unchanged in tumors compared with normal lung tissue (Fig. 6A; Fig. EV4A).
327 Immunohistochemistry confirmed stronger ALKBH2 staining in LUAD than in matched normal
328 samples (Fig. 6B). Consistently, immunoblotting of NSCLC cell lines showed elevated ALKBH2
329 and reduced ALKBH3 relative to BEAS-2B bronchial epithelial cells (Fig. 6C). In survival

330 analyses, high ALKBH2 expression correlated with poorer overall survival, whereas high
331 ALKBH3 correlated with better prognosis (Fig. 6D, E).

332 Because cigarette smoking, a leading cause of lung cancer, also generates alkylating and
333 methylating DNA lesions (Prince, Hammerton et al., 2019), we next examined ALKBH2
334 expression according to smoking status. ALKBH2 transcripts were significantly higher in LUAD
335 patients with a smoking history than in non-smokers (Fig. EV4B). Moreover, MAGEA6, a
336 functional component of the TRIM28–ALKBH2 axis, harbored somatic mutations more
337 frequently in smokers than in non-smokers, whereas MAGEA3 mutations showed no such
338 enrichment (Fig. EV4C). These findings support the notion that ALKBH2 serves as a clinically
339 relevant biomarker linked to smoking-associated alkylation stress and suggest that MAGEA6
340 functions as a potential co-regulator in this pathway.

341 To dissect how TRIM28 and ALKBH2 influence alkylation tolerance, we next employed an
342 acute MMS exposure model. Because prolonged MMS treatment leads to TRIM28 degradation
343 and a delayed increase in ALKBH2, we applied a brief, high-dose MMS pulse (500 μM, 1 h) that
344 induced γ-H2AX while causing limited TRIM28 reduction and minimal change in ALKBH2 levels
345 (Fig. EV4D). Under these conditions, ALKBH2 knockdown using two independent shRNAs
346 reduced proliferation and markedly increased MMS sensitivity (Fig. 6F, G). While TRIM28
347 overexpression had no significant effect on basal proliferation (Fig. EV4E), it enhanced MMS
348 sensitivity, an effect abolished by the RING-inactive C65/68A mutant and reversed by TRIM28
349 re-expression in knockdown cells (Fig. 6H, I). Co-expression of ALKBH2 restored resistance,
350 confirming that ALKBH2 functions as the key downstream effector of TRIM28-mediated
351 cytotoxicity (Fig. 6J).

352 To determine whether MAGEA6 modulates this pathway in a stress-specific manner, we next
353 analyzed its effect on chemosensitivity. MAGEA6 overexpression markedly sensitized H1299
354 cells to MMS, whereas its knockdown conferred resistance; re-expression of MAGEA6 fully
355 restored MMS sensitivity (Fig. EV4F). When TRIM28 was depleted, MAGEA6 no longer
356 enhanced MMS cytotoxicity, and a TRIM28-binding–deficient mutant (D156E/S157Y) exhibited

357 greatly reduced activity (Fig. 6K, L). In contrast, MAGEA6 did not alter sensitivity to cisplatin or
358 to the proteasome inhibitor bortezomib (Fig. EV4G, H), indicating that its regulatory role is
359 specific to alkylation stress. Collectively, these data identify the TRIM28–ALKBH2–MAGEA6
360 axis as a clinically relevant regulatory module that governs cellular tolerance to alkylation damage
361 and links the molecular stress response to chemotherapy outcome.
362

363 **Disruption of the TRIM28-ALKBH2 axis enhances cisplatin cytotoxicity**

364 Acquired chemoresistance remains a major cause of treatment failure in NSCLC. Such resistance
365 often emerges after prolonged drug exposure, activating adaptive DNA repair responses that
366 overlap with mechanisms of platinum resistance (Martin, Hamilton et al., 2008). Consistent with
367 this concept, the TRIM28/*miR*-125b-5p/CREB1 axis has been reported to mediate cisplatin
368 (CDDP) resistance in NSCLC (Tan, Ma et al., 2022). To explore the clinical relevance of TRIM28,
369 we analyzed 771 NSCLC samples. Among treated cases, platinum-based regimens—
370 predominantly CDDP-containing combinations—represented the main therapeutic modality (Fig.
371 EV5A). High TRIM28 expression correlated with poorer overall survival in chemotherapy-treated
372 patients (Fig. EV5B), but not in untreated cases (Fig. EV5C), indicating that TRIM28 functions as
373 a treatment-dependent prognostic factor in NSCLC.

374 Given the clinical association of TRIM28 with chemoresistance, we examined whether
375 sustained DNA damage responses contribute to this phenotype. To this end, we established a
376 chronic MMS exposure model to recapitulate prolonged alkylation stress. In this system, cells were
377 exposed to MMS for 48 h. For dose–response analysis (Fig. 7A), H1299 cells were treated with
378 40–120 μM MMS and analyzed immediately after exposure. For long-term assays (Fig. 7B, C),
379 cells were treated with 100 μM MMS for 48 h, followed by medium replacement and continued
380 culture for an additional 7 days before colony formation analysis. TRIM28 depletion rendered
381 H1299 cells more resistant to MMS, whereas its overexpression in H460 cells increased MMS
382 sensitivity and markedly reduced colony formation. These results demonstrate that TRIM28
383 enhances susceptibility to alkylation-induced cytotoxicity under chronic exposure.

384 To clarify the role of ALKBH2, a downstream effector of TRIM28, in drug sensitivity, we
385 compared MMS and CDDP responses in an ALKBH2-depleted background. Because prolonged
386 MMS exposure induces ALKBH2 upregulation, we used H1299 cells stably knocked down for
387 ALKBH2 to minimize confounding effects. Under these conditions, re-expression of Flag-
388 ALKBH2 increased cell viability upon MMS treatment, confirming its protective role against
389 alkylation damage. At 2 μM, CDDP alone caused minimal cytotoxicity; however, combined
390 MMS–CDDP treatment produced a concentration-dependent increase in cytotoxicity, markedly
391 enhancing MMS-induced cell death. Strikingly, this combination abolished the protective effect
392 of ALKBH2, indicating that CDDP overrides MMS resistance conferred by elevated ALKBH2
393 expression (Fig. 7D).

394 To investigate how CDDP overcomes ALKBH2-mediated MMS resistance, we examined
395 whether oxidative stress and cumulative DNA damage contribute to this effect. As CDDP is known
396 to generate reactive oxygen species, including H_2O_2 (Kim, Lee et al., 2010), we tested whether
397 oxidative stress influences MMS cytotoxicity. Co-treatment of H1299 cells with MMS and
398 increasing H_2O_2 concentrations led to a dose-dependent loss of viability (Fig. EV5D), consistent
399 with the enhanced cytotoxicity observed under combined MMS–CDDP exposure. Alkaline comet
400 assays further showed that low-dose CDDP (2 μM) or MMS (50 μM) alone caused minimal strand
401 breaks, whereas co-treatment markedly increased tail moments (Fig. 7E; $p < 0.001$). These
402 findings suggest that oxidative and alkylating stress act cooperatively to exacerbate DNA damage,
403 thereby counteracting ALKBH2-mediated protection.

404 To define subtoxic MMS concentrations suitable for combination therapy, we determined IC_{50}
405 values in H1299 and H460 cells, which were approximately 141.5 μM and 236.8 μM, respectively
406 (Fig. EV5F). Subsequent assays used MMS doses below these IC_{50} values to minimize single-
407 agent toxicity. Under these conditions, low-dose MMS significantly reduced the IC_{50} of CDDP in
408 both H1299 and H460 cells (Fig. 7F, G), demonstrating that prior alkylation stress sensitizes cells
409 to cisplatin. In colony formation assays, combined MMS and CDDP treatment markedly
410 suppressed clonogenic survival (Fig. 7H, I). In three-dimensional (3D) tumor spheroids, the

411 combination similarly reduced spheroid size and viability, accompanied by pronounced
412 morphological collapse and decreased Calcein-AM fluorescence, indicating a loss of viable cells
413 (Fig. 7J, K). Collectively, these findings demonstrate that combined alkylation and platinum
414 treatments synergistically enhance DNA damage and cytotoxicity in NSCLC cells. Furthermore,
415 they support a model in which persistent alkylation stress disrupts the TRIM28–ALKBH2
416 regulatory equilibrium, thereby increasing cellular susceptibility to platinum-based chemotherapy.

417 **DISCUSSION**

418 Building on our previous work showing that the deubiquitinase OTUD4 noncanonically stabilizes
419 the alkylation repair enzymes ALKBH2 and ALKBH3 (Zhao et al., 2015), this study defines the
420 opposing ubiquitination arm of this repair pathway. Proteomic profiling of the alkylation-
421 responsive ASCC complex—functionally linked to ALKBH3 and also detected in association with
422 ALKBH2 (Brickner et al., 2017)—identified TRIM28 as an ASCC2-associated component,
423 implicating a connection between transcriptional regulators and ubiquitin signaling during
424 alkylation repair. Consistent with this link, we identified TRIM28, in cooperation with the cancer-
425 testis antigen MAGEA6, as an E3 ligase complex that regulates ALKBH2 stability through K48-
426 linked ubiquitination and proteasomal degradation (Fig. 1–3). Under basal conditions, the
427 TRIM28–MAGEA6 complex maintains steady-state ALKBH2 turnover, while ALKBH2
428 enhances TRIM28 transcription, forming a feedback loop that supports repair homeostasis. Upon
429 alkylation stress, this feedback loop undergoes dynamic reprogramming. During acute MMS
430 exposure, TRIM28–ALKBH2 binding is strengthened, leading to accelerated ALKBH2
431 degradation, whereas prolonged exposure redirects ubiquitination toward TRIM28, resulting in its
432 degradation and the subsequent stabilization and transcriptional induction of ALKBH2 (Fig. 8).

433 This study identifies TRIM28, together with the cancer-testis antigen MAGEA6, as the E3
434 ligase complex responsible for ALKBH2 ubiquitination and proteasomal turnover, defining the
435 first ubiquitin-dependent mechanism known to regulate ALKBH2 stability. This regulatory
436 module also clarifies how substrate specificity, DNA-engagement–dependent accessibility, and
437 reciprocal feedback regulation are integrated within the ALKBH2 control system. The AlkB
438 family of demethylases is involved in multiple steps of nucleic acid repair (Xu & Bochtler, 2020),
439 yet their post-translational regulation remains poorly understood. Distinct E3 ligases have been
440 identified for other AlkB family members, including TRIM28 for ALKBH5 (Meng et al., 2025)
441 and TRIM21 for FTO (Zhang et al., 2025); however, the mechanism regulating ALKBH2 turnover
442 remains undefined. Notably, unlike canonical MAGE–TRIM interactions (Jin, Pan et al., 2017,
443 Pineda & Potts, 2015), MAGEA6 functions both as a scaffolding cofactor for TRIM28 and as a

444 direct binding partner of ALKBH2 (Fig. 3B), suggesting a dual-binding mode that enhances
445 substrate specificity under alkylation stress. Although ALKBH2 and ALKBH3 share conserved
446 catalytic cores, TRIM28 preferentially associates with ALKBH2 (Fig. 1I). This selectivity reflects
447 the unique hairpin (finger) motif and flexible long-loop region of ALKBH2—structural elements
448 required for DNA engagement (Yang et al., 2008). Importantly, docking analysis predicts that the
449 TRIM28–ALKBH2 contact region lies near the DNA-binding surface of ALKBH2 (Fig. 1J), and
450 ssDNA competitively reduces their association (Fig. 1K). These observations support a model in
451 which DNA engagement transiently restricts TRIM28 access to ALKBH2, thereby coupling
452 catalytic activity with subsequent ubiquitin-dependent turnover once DNA dissociates. Moreover,
453 under basal conditions, ALKBH2 enhanced TRIM28 expression at both mRNA and protein levels
454 (Fig. 2J–L), thereby forming the transcriptional arm of this feedback loop. This regulation is
455 consistent with previous findings that ALKBH2 modulates promoter methylation and transcription
456 of other targets, including MGMT and BMI1 (Ke, Ye et al., 2020, Malacrida, Di Domizio et al.,
457 2022). Together with previous evidence that the deubiquitinase OTUD4 associates with both
458 ALKBH2 and ALKBH3 (Zhao et al., 2015), these data delineate a reciprocal ubiquitin loop in
459 which TRIM28–MAGEA6-mediated ubiquitination counterbalances OTUD4-dependent
460 deubiquitination, thereby maintaining ALKBH2 homeostasis.

461 TRIM28 is itself regulated under alkylation stress, introducing a second layer of control within
462 the TRIM28–ALKBH2 pathway. MMS uniquely triggered K48-linked polyubiquitination and
463 proteasomal degradation of TRIM28 (Fig. 5A–G), whereas other genotoxic agents—including
464 temozolomide (TMZ), cisplatin (CDDP), and H_2O_2—did not induce TRIM28 modification or loss
465 (Fig. 5H; Fig. EV3D–F). Instead, these agents produced distinct TRIM28-independent effects on
466 ALKBH2: TMZ increased ALKBH2 protein abundance without reducing TRIM28 levels (Fig.
467 EV3D), H_2O_2 reduced ALKBH2 (Fig. EV3F), and CDDP caused no appreciable changes (Fig.
468 EV3E). The TMZ-driven increase in ALKBH2 aligns with previous reports of transcriptional
469 induction in glioblastoma cells (Johannessen et al., 2013), indicating that TMZ primarily engages
470 a transcriptional, rather than a TRIM28-dependent post-translational, regulatory mechanism.

471 MMS-induced ubiquitination of TRIM28 was substantially reduced in the K554/779/804R mutant
472 (Fig. 5I), which targets the major SUMO-acceptor lysines of TRIM28 (Ivanov et al., 2007),
473 suggesting that MMS-triggered ubiquitination may occur at, or be influenced by, this lysine cluster.
474 Conversely, interaction with TRIM24 further enhanced TRIM28 ubiquitination upon MMS
475 treatment, suggesting that TRIM24 facilitates this process under alkylation stress. This stress-
476 specific turnover contrasts with the RNF4-mediated degradation of phosphorylated and
477 SUMOylated TRIM28 reported in the double-strand break response (Kuo et al., 2014), indicating
478 that different forms of genotoxic stress engage distinct ubiquitin pathways. Consistent with this
479 notion, alkylation damage triggers specialized ubiquitin responses—for example, MMS promotes
480 HLTF degradation without affecting UV-induced PCNA monoubiquitination (Lin, Zeman et al.,
481 2011), and also activates the E3 ligase RNF113A to mediate recruitment of the ASCC–ALKBH3
482 repair complex (Tsao, Brickner et al., 2021). Collectively, these observations place TRIM28
483 within a broader framework of alkylation-specific ubiquitin regulation, indicating that MMS
484 engages a distinct ubiquitin signaling route that couples targeted protein turnover to DNA repair
485 adaptation. Notably, TRIM24 has been reported to cooperate with TRIM28 in transcriptional
486 programs across multiple cancers, where TRIM28 both stabilizes TRIM24 and promotes its
487 transcriptional activity (Fong, Zhao et al., 2018, Herquel, Ouararhni et al., 2011). In contrast, in
488 our system TRIM24 enhanced TRIM28 ubiquitination and promoted its degradation in response
489 to MMS treatment, indicating a stress-induced reversal of their regulatory relationship. This MMS-
490 selective mechanism limits TRIM28 stability and may facilitate the remodeling of repair-
491 associated chromatin complexes under prolonged alkylation stress.

492 A key mechanistic insight from this study is the discovery of a time-resolved TRIM28–
493 ALKBH2 feedback loop that dynamically modulates DNA repair during alkylation stress. This
494 loop functions as a biphasic molecular switch, acting sequentially to balance repression and
495 activation phases. During acute MMS exposure, TRIM28 binds ALKBH2 to promote its K48-
496 linked ubiquitination and proteasomal degradation, thereby transiently restraining repair capacity
497 (Fig. 4). As MMS exposure persists, TRIM28 undergoes ubiquitination and degradation, whereas

498 ALKBH2 becomes stabilized and transcriptionally induced (Fig. 4-5), thereby marking a temporal
499 transition from repression to activation of repair capacity. This transition parallels the functional
500 switch in demethylation repair, where ALKBH2 catalyzes the oxidative demethylation of damaged
501 bases. This biphasic switch exemplifies a general principle of stress adaptation, reminiscent of the
502 time-delayed feedback observed in the ATM–TRIM28 (KAP1) and p53–MDM2 circuits, which
503 coordinate DNA repair and checkpoint recovery (Jaiswal, Benada et al., 2017, Wang, Ivanov et
504 al., 2005). Unlike these canonical pathways, the TRIM28–ALKBH2 module integrates ubiquitin-
505 and transcription-linked feedback loops, thus enabling the E3 ligase and its substrate to function
506 as reciprocal regulators. Under basal conditions, ALKBH2 sustains TRIM28 expression at both
507 mRNA and protein levels (Fig. 2J–L), thereby maintaining repair homeostasis. Prolonged
508 alkylation stress, however, leads to TRIM28 depletion and ALKBH2 accumulation, thereby
509 disrupting this balance and shifting the system toward enhanced repair capacity and increased
510 tolerance to persistent damage. Such a biphasic regulatory mechanism may enable cells to fine-
511 tune repair activity according to the duration and intensity of alkylation stress, thereby enhancing
512 DNA repair adaptability during chemotherapy.

513 Clinically, the TRIM28–ALKBH2 regulatory loop emerges as a relevant determinant of
514 NSCLC chemotherapy response. ALKBH2 is frequently upregulated in lung adenocarcinoma and
515 correlates with poorer overall survival (Fig. 6A–D), consistent with its function in counteracting
516 DNA alkylation damage (Duncan et al., 2002, Feng et al., 2022). By contrast, TRIM28 correlates
517 with patient outcome only in chemotherapy-treated cohorts (Fig. EV5A-C), suggesting that its
518 regulatory activity becomes functionally engaged under therapeutic stress. MAGEA6 mutations,
519 which are enriched in smokers (Fig. EV4C), may link smoking-induced alkylation stress to
520 disruption of this proteolytic module. Mechanistically, TRIM28 functions as the cognate E3 ligase
521 for ALKBH2, with MAGEA6 serving as its scaffolding adaptor, together forming a ubiquitin-
522 mediated checkpoint that modulates repair dynamics under chemotherapeutic stress (Figs. 1–3).
523 Functionally, TRIM28 overexpression increased MMS sensitivity, whereas ALKBH2 re-
524 expression reversed this effect (Fig. 6F–I), indicating that ALKBH2 acts as the primary effector

525 of TRIM28-dependent cytotoxicity. Combining MMS with cisplatin enhanced DNA damage,
526 suppressed clonogenic survival, and overcame ALKBH2-mediated alkylation tolerance, resulting
527 in synergistic cytotoxicity (Fig. 7B–K). Notably, although TRIM28 has been implicated in
528 promoting NSCLC chemoresistance through mechanisms such as *miR*-125b-5p/CREB1 signaling,
529 E2F1 regulation, and DNA-damage control (Ginn, Maltas et al., 2023, Liu, Xiao et al., 2017,
530 Lundholm, Hååg et al., 2013, Saxena, Quan et al., 2025, Tan et al., 2022), it instead enhanced
531 cytotoxicity by promoting ALKBH2 degradation in our MMS-based system. This context
532 dependence likely reflects the mechanistic distinction between alkylation stress and platinum-
533 induced DNA crosslinking. Prolonged MMS exposure results in TRIM28 degradation
534 accompanied by increased ALKBH2 expression (Fig. 5A–H; Fig. EV3D–F), suggesting an
535 adaptive enhancement of DNA repair capacity during sustained alkylation stress. Although this
536 adaptation may confer partial tolerance to MMS, the concomitant loss of TRIM28 could sensitize
537 cells to platinum, consistent with the synergistic cytotoxicity observed under combined treatment
538 (Fig. 7D–K). Clinically, these findings are consistent with patient data showing that TRIM28
539 acquires prognostic significance during chemotherapy, where high expression correlates with
540 poorer overall survival. This association supports a potential therapeutic rationale for combining
541 alkylating and platinum agents in tumors with elevated TRIM28 expression.

542 In summary, this study delineates a stress-dependent TRIM28–ALKBH2 feedback loop that
543 modulates alkylation repair capacity in NSCLC cells. Under basal conditions, the TRIM28–
544 MAGEA6 complex mediates K48-linked polyubiquitination and proteasomal turnover of
545 ALKBH2. Acute MMS exposure enhances assembly of the TRIM28–ALKBH2 complex and
546 promotes ALKBH2 degradation, whereas prolonged MMS exposure induces K48-linked
547 ubiquitination of TRIM28 and its proteasomal degradation, leading to ALKBH2 stabilization and
548 transcriptional upregulation. This stress-responsive circuit integrates post-translational
549 mechanisms with transcriptional control of ALKBH2, thereby collectively modulating cellular
550 responses to alkylating agents. The upstream cues that initiate TRIM28 degradation and their
551 coordination with transcriptional programs remain to be clarified. Future studies using patient-

552 derived and *in vivo* systems will provide further insight into defining these mechanisms and
553 assessing their relevance to chemotherapy response in NSCLC.

554 **Methods**

555 **Reagents and tools table**

Reagent/Resource	Reference or Source	Identifier or Catalog Number
Cell Lines		
HEK293T (*H. sapiens*)	ATCC	CRL-11268
NCI-H1299 (*H. sapiens*)	Cell Bank of the Chinese Academy of Sciences	SCSP-589
A549 (*H. sapiens*)	Cell Bank of the Chinese Academy of Sciences	SCSP-503
NCI-H460 (*H. sapiens*)	Cell Bank of the Chinese Academy of Sciences	SCSP-584
Antibodies		
Rabbit anti-TRIM28	Proteintech	Cat #15202-1-AP
Mouse anti-ALKBH2	Sigma-Aldrich	Cat #A8228
Rabbit anti-HA	Proteintech	Cat #51064-2-AP
Mouse anti-Flag	Sigma-Aldrich	Cat #F3165
Mouse anti-Myc	Millipore	Cat #05-419
Mouse anti-His	Proteintech	Cat #66005-1-Ig
Mouse anti-MBP	New England Biolabs	Cat #E8030S
Rabbit anti-MAGEA3/6	Zenbio Science	Cat #R24906
Rabbit anti-TRIM24	Zenbio Science	Cat #R27382
Rabbit anti-ALKBH3	Millipore	Cat #09-882
Rabbit anti-MGMT	Proteintech	Cat #17195-1-AP
Mouse anti-P53	Santa Cruz	Cat #sc-126
Rabbit anti-γ-H2AX	Abmart	Cat #T56572
Rabbit anti-H2AX	Cusabio	Cat #Ab-142
Rabbit anti-K48-Ubiquitin	Millipore	Cat #05-1307
Mouse anti-ubiquitin	Santa Cruz	Cat #sc-8017
Rabbit anti-PSMD4	Selleck	Cat #F1309
Rabbit anti-PSMB5	Selleck	Cat #F1421
HRP-conjugated β-actin	Genscript Biotech	Cat #A00730

HRP-conjugated β-tubulin	Earthox	Cat #E021043
HRP-conjugated anti-rabbit	Proteintech	Cat #SA00001-2
HRP-conjugated anti-mouse	Proteintech	Cat #SA00001-1
Alexa Fluor 488 goat anti-mouse	Thermo Fisher Scientific	Cat #A-11029
Alexa Fluor 594 goat anti-rabbit	Thermo Fisher Scientific	Cat #A-11037
Recombinant DNA		
pHAGE-puro-Flag-TRIM28	This study	N/A
pHAGE-puro-3xHA-TRIM28	This study	N/A
pHAGE-puro-His-TRIM28	This study	N/A
pMSCV-puro-TAP-TRIM28	This study	N/A
pHAGE-puro-Flag-ALKBH2	This study	N/A
pHAGE-blast-HA-ALKBH2	This study	N/A
pMSCV-blast-TAP-ALKBH2	This study	N/A
pCMV-Flag-TRIM24	This study	N/A
pCMV-Flag-ALKBH2	This study	N/A
pCMV-Flag-ALKBH2 H171/D173A	This study	N/A
pCMV-Flag-ALKBH3	This study	N/A
pCMV-Flag-MGMT	This study	N/A
pHAGE-puro-Flag-MAGEA6	This study	N/A
pHAGE-puro-Flag-MAGEA6 Mut	This study	N/A
pCMV-Myc-MAGEA6	This study	N/A
pLKO.1 puro	Addgene	Cat #8453
lentiCRISPR v2	Addgene	Cat #52961
pcDNA3.1-HA-ub	Zhao et al., 2015	N/A
pRK5-HA-ub K48-only	Zhao et al., 2015	N/A
pRK5-HA-ub K48R	Zhao et al., 2015	N/A
psPAX2	Zhao et al., 2015	N/A
pMD2.G	Zhao et al., 2015	N/A
pENTR-4	Zhao et al., 2015	N/A
pHAGE-CMV-Flag/HA/His	Zhao et al., 2015	N/A
Oligonucleotides and other sequence-based reagents		

ssDNA	This study	CAAAGCTTCCGAGTAC TTGCAGCTG
shTRIM28, shALKBH2, shMAGEA6, sgTRIM28	This study	Appendix Table S3
qPCR Primer	This study	Appendix Table S4
Chemicals, Enzymes and other reagents		
Cell Culture & Transfection		
Fetal bovine serum (FBS)	Gibco	Cat #10099-141C
Dulbecco's modified Eagle's medium (DMEM)	Gibco	Cat #C11995500BT
Penicillin-streptomycin	Gibco	Cat #15140122
0.25%Trypsin-EDTA	Gibco	Cat #C25200-072
Polybrene	Sigma-Aldrich	Cat #28728-55-4
Lipo8000™ Transfection Reagent	Beyotime	Cat #C0533
Chemicals, Inhibitors & Drugs		
Cycloheximide	Cell Signaling Technology	Cat #2112
Methyl methanesulfonate	Sigma-Aldrich	Cat #129925
Cisplatin	MedChemExpress	Cat #HY-17394
Temozolomide	Selleck	Cat #S1237
Bortezomib	MedChemExpress	Cat #HY-10227
Ascorbic acid	Shanghai Hu Shi	Cat #10004014
Protease inhibitor cocktail	Beyotime	Cat #P1051
Immunoprecipitation & Affinity Purification		
Anti-Flag M2-agarose beads	Sigma-Aldrich	Cat #L00425
Protein A/G Magnetic Beads	Selleck	Cat #B23202
Anti-HA magnetic beads	Selleck	Cat #B26201
HaloLink™ resin	Promega	Cat #G1915
Amylose Resin	New England Biolabs	Cat #E8021S
Molecular Biology		
Gateway™ LR Clonase™ II Enzyme mix	Invitrogen	Cat #11791020
RNAeasy™ RNA Isolation Kit	Beyotime	Cat #R0026

SYBR qPCR Mix	Tsingke	Cat #TSE501
Assays & Kits		
CCK8 assay	ApexBio	Cat #K1018
Comet Assay Kit	Keygentec	Cat #KGA1302
Myco-Lumi Luminescent Mycoplasma Detection Kit	Beyotime	Cat #C0297S
Silver Staining Kit	Sangon Biotech	Cat #C500021
Staining, Imaging & Fixation		
DAPI	Beyotime	Cat #C1002
Hoechst 33342	BD Biosciences	Cat #561908
Calcein/PI Live/Dead Assay	Beyotime	Cat #C2015S
4% paraformaldehyde	Beyotime	Cat #P0099
0.1% crystal violet	Beyotime	Cat #C0121
Software		
GraphPad Prism	https://www.graphpad.com	Version 9.5.0
Pymol	https://pymol.org/	Version 2.6.0a0
RStudio	https://posit.co/	Version 4.4.2
ImageJ	https://imagej.en.softonic.com	Version 1.54K

Methods and protocols

Cell culture

Cells were maintained in Dulbecco's modified Eagle's medium (DMEM) supplemented with 10% heat-inactivated fetal bovine serum and penicillin–streptomycin. Cultures were maintained at 37 °C in a humidified atmosphere containing 5% CO_2. All experiments were performed using low-passage cells (passages 5–15). Mycoplasma contamination was routinely monitored using a luminescence-based detection assay.

Plasmid constructs, mutagenesis, and viral infection

Full-length human TRIM28 and ALKBH2 cDNAs were used as templates for PCR-based site-directed mutagenesis. TRIM28 deletion and point mutants (including BCC, residues 141–400, and the RING-inactive C65/68A variant) were generated by PCR, cloned into pENTR-4, and

569 transferred into pHAGE-CMV-Flag/HA/His through Gateway LR recombination. ALKBH2
570 variants were cloned into pCMV-Flag for mammalian expression and into pET28a-His-2×Flag for
571 bacterial expression. All constructs were verified by Sanger sequencing. MAGEA6 wild-type
572 cDNA, obtained by reverse transcription of A549 RNA, and H1299-derived MAGEA6 variants
573 were generated analogously. Transient transfections were performed using Lipo8000.
574 Lentiviruses were produced in HEK293T cells by co-transfecting pLKO.1 or pHAGE vectors
575 with the packaging plasmids psPAX2 and pMD2.G. Viral supernatants were collected at 48–72 h,
576 clarified, and filtered through 0.45-μm membranes. Target cells were infected in the presence of
577 polybrene (6 μg/mL) for 12 h. Stable cell lines were selected with puromycin (1 μg/mL) or
578 blasticidin (5 μg/mL) for 3 days and maintained thereafter.
579
580 ***shRNA and CRISPR/Cas9 knockdown/knockout***
581 For shRNA-mediated knockdown, annealed oligonucleotides encoding target-specific sequences
582 were cloned into the pLKO.1 vector and packaged into lentiviral particles in HEK293T cells.
583 Target cells were transduced and selected with puromycin for 3 days to establish stable knockdown
584 lines. Knockdown efficiency was confirmed by western blotting (WB). A non-targeting shRNA
585 was used as a control.
586 For CRISPR/Cas9-mediated knockout of TRIM28, single-guide RNAs (sgRNAs) were
587 designed according to established criteria and cloned into the lentiCRISPRv2 vector. Lentiviral
588 particles were produced in HEK293T cells and used to transduce target cells, followed by
589 puromycin selection. Single-cell clones were generated by limiting dilution, and successful
590 knockout was verified by WB. All oligonucleotide sequences are listed in Appendix Table S3.
591
592 ***Immunoprecipitation and western blotting***
593 For overexpression immunoprecipitation (IP), HEK293T cells were transfected with the indicated
594 plasmids using Lipo8000 and cultured for 2–3 days before lysis. Cells were lysed in buffer
595 containing 150 mM NaCl, 50 mM Tris-HCl (pH 7.9), 1% Triton X-100, 10% glycerol, and 2 mM

596 DTT supplemented with protease and phosphatase inhibitors. Clarified lysates were incubated
597 overnight at 4 °C with anti-Flag M2-agarose beads or anti-HA-agarose beads. For denaturing IP,
598 lysates were boiled in TBS containing 1% SDS and diluted with lysis buffer to a final concentration
599 of 0.1% SDS before IP.

600 For endogenous IP from H1299 cells, lysates were prepared in the same buffer and cleared by
601 centrifugation (15,000 × *g*, 10 min, 4 °C). Supernatants were pre-cleared with Protein A/G
602 magnetic beads for 1 h and incubated overnight at 4 °C with anti-TRIM28 (1.5 μg). Immune
603 complexes were captured with Protein A/G magnetic beads, washed in lysis buffer, and eluted in
604 Laemmli buffer. Input and flow-through fractions were analyzed in parallel by WB to verify
605 expression and loading.

606 For ssDNA competition assays, purified Flag-ALKBH2 was added to HEK293T whole-cell
607 lysates supplemented with synthesized single-stranded DNA (ssDNA) oligonucleotides and
608 incubated overnight at 4 °C. Disruption of the TRIM28–ALKBH2 interaction was assessed by
609 Flag IP, followed by WB.

610 For WB, proteins were separated by SDS–PAGE and transferred to PVDF membranes.
611 Membranes were blocked with 5% non-fat milk in TBST for 1 h at room temperature, incubated
612 with primary antibodies overnight at 4 °C, and then with HRP-conjugated secondary antibodies
613 for 1–1.5 h at room temperature. Signals were detected using enhanced chemiluminescence (ECL).
614

615 ***In vitro MBP pull-down assay***

616 Recombinant maltose-binding protein (MBP)–tagged TRIM28 (MBP–TRIM28), MBP–
617 MAGEA6, MBP alone, and His–Flag–tagged ALKBH2 (His–Flag–ALKBH2) were expressed in
618 *E. coli* Rosetta (DE3). Protein expression was induced with IPTG according to standard procedures.
619 Bacterial pellets were collected and lysed, and MBP fusion proteins were purified using amylose
620 resin.

621 For pull-down assays, purified MBP–TRIM28, MBP–MAGEA6, or MBP alone was
622 immobilized on amylose resin and washed with binding buffer. The resin was then incubated with

623 purified His–Flag–ALKBH2 at 4 °C with gentle rotation. After extensive washing, bound proteins
624 were eluted by boiling in Laemmli sample buffer and analyzed by WB using anti-His or anti-Flag
625 antibodies.
626
627 ***Immunofluorescence (IF)***
628 Cells grown on glass coverslips were treated as indicated, fixed in 4% paraformaldehyde for 30
629 min, and permeabilized with 0.5% Triton X-100 in PBS for 15 min at room temperature. After
630 washing with PBST, samples were incubated with primary antibodies overnight at 4 °C. The
631 following day, coverslips were washed and incubated with fluorophore-conjugated secondary
632 antibodies together with Hoechst 33342 or DAPI for 1.5 h at 37 °C. Coverslips were mounted and
633 imaged using an Olympus fluorescence microscope. Colocalization analysis was performed using
634 ImageJ, and Pearson correlation coefficients were calculated when required.
635
636 ***Cycloheximide chase assay***
637 For cycloheximide (CHX) chase assays, cells were treated with 150 μg/mL CHX for the indicated
638 durations. Cells were harvested at each time point and analyzed by WB to assess protein stability.
639
640 ***RNA isolation and qRT-PCR***
641 Total RNA was isolated using the RNAeasy™ RNA Isolation Kit, following the manufacturer's
642 instructions. RNA concentration and purity were assessed using a NanoDrop spectrophotometer
643 (Thermo Fisher Scientific) by measuring absorbance at 260 nm and calculating the A260/A280
644 and A260/A230 ratios. First-strand cDNA synthesis was performed using the BeyoFast™ cDNA
645 Synthesis Kit, followed by qPCR using the BeyoFast™ SYBR Green qPCR Mix, according to the
646 manufacturer's guidelines. Gene expression levels were normalized to *β-actin* as an internal
647 control. All qRT-PCR primer sequences are listed in Appendix Table S4.

648 ***Protein–protein docking and structural modeling***
649 The tertiary structures of human ALKBH2 (PDB ID: 3BTZ), ALKBH3 (PDB ID: 2NCU), and the

650 RBCC domain of TRIM28 (PDB ID: 6QAJ) were retrieved from the Protein Data Bank
651 (http://www.rcsb.org). Protein–protein docking simulations were conducted using the GRAMM-
652 X web server (http://gramm.compbio.ku.edu). Predicted complex interfaces between TRIM28 and
653 MAGEA6 were modeled using AlphaFold3 (https://alphafoldserver.com/). The resulting docking
654 complexes were visualized and analyzed using PyMOL.

655 ***Mass spectrometry***

656 TRIM28 complexes from H1299 cells stably expressing TAP-TRIM28 were immunoaffinity-
657 purified using Flag M2 beads, eluted with Flag peptide, separated by SDS–PAGE, and visualized
658 by silver staining. Afterward, samples were analyzed by LC–MS/MS. Mass spectrometry was
659 performed by Shanghai Baipu Company utilizing an Easy nLC 1200 system (Thermo Fisher
660 Scientific) with a Dr. Maisch GmbH column (75 μm × 150 mm, 3 μm C18) for gradient separation.
661 Data-dependent acquisition (DDA) MS was performed on a Q-Exactive HF-X mass spectrometer
662 (Thermo Fisher Scientific). Peptides were matched against the UniProt Reference proteome *Homo*
663 *sapiens* (Human) [9606] database (81791-20230317.fasta), obtained from
664 https://www.uniprot.org/proteomes/UP000005640.

665

666 ***Affinity purification of K48-linked polyubiquitinated proteins (Halo-TUBE)***

667 K48-linked ubiquitin chains and ubiquitinated proteins were isolated from cell extracts using a
668 tandem ubiquitin-binding entity (TUBE) containing Halo-tag (Halo-TUBE) resin under denaturing
669 conditions. Briefly, cells were harvested, lysed, and denatured by boiling in TBS containing 1%
670 SDS, then diluted with lysis buffer to reduce SDS concentration to 0.1% before affinity
671 purification. Extracts were incubated with 10 μL of HaloLink™ resin (Promega) pre-bound to
672 purified Halo-TUBE protein (10 μg per sample). The clarified extracts were incubated with Halo-
673 TUBE-bound resin overnight at 4 °C with rotation. Subsequently, the resin was washed five times
674 with washing buffer, boiled in Laemmli sample buffer, and analyzed by WB.

675

676 ***Cell proliferation, CDDP sensitivity, and synergy assays***

677 For the MMS Sensitivity Assay, cells (2,000–5,000 per well, in 96-well plates) were exposed to
678 high-concentration methyl methanesulfonate (MMS; 200–800 μM) for 1 h at 37 °C, followed by
679 replacement with fresh medium, or low-concentration MMS (0–200 μM) continuously for 48 h.
680 Cell viability was assessed at 48 h using the CCK-8 assay. For the Cisplatin Sensitivity Assay,
681 cells were treated with cisplatin (CDDP; 0–40 μM) for 48 h, and cell viability was measured using
682 the CCK-8 assay. The half-maximal inhibitory concentration (IC_{50}) was calculated using
683 GraphPad Prism software. For the Synergy Assay, cells were treated with cisplatin (CDDP) alone
684 or in combination with low-concentration MMS for 48 h. Cell viability was quantified using the
685 CCK-8 assay.

686

687 ***Colony formation assay***

688 To assess clonogenic survival, H460 cells were seeded in 24-well plates (400 cells per well) and
689 incubated overnight to allow cell attachment. The following day, DMSO (vehicle control) or MMS
690 was added to each well at the indicated concentrations. For combination treatment, the medium
691 was replaced with fresh medium after 48 h of treatment with MMS alone, cisplatin (CDDP) alone,
692 or their combination. After 5–10 days of incubation to allow colony formation, the medium was
693 removed, and cells were fixed with 4% paraformaldehyde for 10 minutes at room temperature.
694 Following fixation, cells were stained with 0.1% crystal violet according to the manufacturer's
695 instructions. Plates were washed three times with distilled water, air-dried, and the number of
696 colonies was counted.

697 ***Alkaline comet assay***

698 Alkaline single-cell agarose gel electrophoresis (comet) assays were performed using a Comet
699 Assay Kit, following the manufacturer's instructions. Comet images were visualized using an
700 Olympus fluorescence microscope (Olympus Corporation). The percentage of DNA in the tail
701 (Tail DNA%) and the Tail Moment were quantified using ImageJ software with the Comet Assay
702 plugin. Tail DNA% was calculated as: Tail DNA% = (Tail DNA Intensity / (Tail DNA Intensity

703 + Head DNA Intensity)) × 100%, and the Tail Moment was calculated as: Tail Moment = Tail
704 Length × Tail DNA%.

705 ***3D tumorsphere culture***

706 H1299 cells (~2,000 cells per drop) were cultured as hanging drops for 72 hours to facilitate
707 spheroid formation and then transferred to ultra-low attachment 96-well plates (LV-ULA002-
708 96UW, Liver Biotech). Tumor spheres were subsequently exposed to the indicated concentrations
709 of MMS and/or cisplatin (CDDP) for 48 hours. After drug exposure, the culture medium was
710 replaced, and spheroids were cultured for an extended period (up to 3–4 weeks). Tumorsphere
711 viability and cytotoxicity were assessed using a Calcein-AM/Propidium Iodide (PI) Live/Dead
712 assay kit. Fluorescence images distinguishing live (green) and dead (red) cells were acquired using
713 an Olympus fluorescence microscope (Olympus Corporation).

714 ***Bioinformatics and clinical data analysis***

715 Clinical data for TCGA patients with LUAD and LUSC were obtained from the TCGA data portal
716 (https://tcga-data.nci.nih.gov/tcga/). Gene expression data from TCGA and protein expression data
717 from CPTAC were analyzed using ULCAN. Survival analysis was performed using the Kaplan–
718 Meier Plotter (http://kmplot.com/analysis) with default settings for overall survival, and hazard
719 ratios and log-rank p-values were reported. Images of ALKBH2 immunohistochemistry (IHC)
720 were downloaded from the Human Protein Atlas (http://www.proteinatlas.org).
721 MAGEA6/MAGEA3 mutations were surveyed using COSMIC (http://cancer.sanger.ac.uk/cosmic)
722 and cBioPortal (http://www.cbioportal.org). Cutoffs and covariates are specified in the
723 corresponding figure legends.

724 ***Statistical analysis***

725 All graphs and statistical analyses were performed using GraphPad Prism version 9.5.0. Data are
726 presented as means ± standard deviation (SD) from at least three independent experiments ($n \geq 3$).
727 Statistical significance was determined using an unpaired, two-tailed Student's t-test. P values <
728 0.05 were considered significant (*$p < 0.05$, **$p < 0.01$).

Author contributions

Zhiming Sun: Writing – original draft, Visualization, Resources, Investigation, Data curation. **Yunfang Deng:** Formal analysis, Investigation, Data curation. **Yue Liu:** Investigation. **Zhaohui Liu:** Visualization, Formal analysis. **Jiabing Li:** Visualization, Formal analysis. **Lihui Wu:** Investigation. **Liyuan Zeng, Xiaorong Feng, Lin Miao:** Investigation, Data curation. **Ying Sheng, Bei Chen, Yuming He, Ye Liu:** Investigation. **Yu Zhao:** Writing – review & editing, Visualization, Supervision, Funding acquisition, Conceptualization.

Disclosure and competing interests statement

The authors declare that they have no competing interests.

Data availability

All data supporting the findings of this study are available within the article and its Supplementary Information.

Acknowledgments

This work was supported by the National Natural Science Foundation of China (31971232) and the Natural Science Foundation of Hunan Province (2019JJ40185) to YZ.

References

Brickner JR, Soll JM, Lombardi PM, Vagbo CB, Mudge MC, Oyeniran C, Rabe R, Jackson J, Sullender ME, Blazosky E et al. (2017) A ubiquitin-dependent signalling axis specific for ALKBH-mediated DNA dealkylation repair. *Nature* 551: 389-393

Bu X, Qu X, Guo K, Meng X, Yang X, Huang Q, Dou W, Feng L, Wei X, Gao J et al. (2021) CD147 confers temozolomide resistance of glioma cells via the regulation of β-TrCP/Nrf2 pathway. *International journal of biological sciences* 17: 3013-3023

Chang G, Xie GS, Ma L, Li P, Li L, Richard HT (2023) USP36 promotes tumorigenesis and drug sensitivity of glioblastoma by deubiquitinating and stabilizing ALKBH5. *Neuro Oncol* 25: 841-853

Chen Y, Pang W, Ma G, Yan Y, Xiao Z, Chen Y, Ding Z, Chen L, Hou X, Cao H (2025) March5-mediated Trim28 degradation preserves islet β-cell function in mice. *Nature communications* 16: 7073

Chen Z, Zhou Y, Xue C, Zeng L, Deng S, Xu Z, Li M, Zhao H, He X, Liu S et al. (2025) Psychological stress-induced ALKBH5 deficiency promotes tumour innervation and pancreatic cancer via extracellular vesicle transfer of RNA. *Nat Cell Biol* 27: 1035-1047

Cui YH, Wei J, Fan H, Li W, Zhao L, Wilkinson E, Peterson J, Xie L, Zou Z, Yang S et al. (2024) Targeting DTX2/UFD1-mediated FTO degradation to regulate antitumor immunity. *Proceedings of the National Academy of Sciences of the United States of America* 121: e2407910121

Czerwińska P, Mazurek S, Wiznerowicz M (2017) The complexity of TRIM28 contribution to cancer. *Journal of biomedical science* 24: 63

Dai W, Tian R, Yu L, Bian S, Chen Y, Yin B, Luan Y, Chen S, Fan Z, Yan R et al. (2024) Overcoming therapeutic resistance in oncolytic herpes virotherapy by targeting IGF2BP3-induced NETosis in malignant glioma. *Nature communications* 15: 131

Doyle JM, Gao J, Wang J, Yang M, Potts PR (2010) MAGE-RING protein complexes comprise a family of E3 ubiquitin ligases. *Molecular cell* 39: 963-74

Drabløs F, Feyzi E, Aas PA, Vaagbø CB, Kavli B, Bratlie MS, Peña-Diaz J, Otterlei M, Slupphaug G, Krokan HE (2004) Alkylation damage in DNA and RNA--repair mechanisms and medical significance. *DNA Repair (Amst)* 3: 1389-407

Duncan T, Trewick SC, Koivisto P, Bates PA, Lindahl T, Sedgwick B (2002) Reversal of DNA alkylation damage by two human dioxygenases. *Proceedings of the National Academy of Sciences of the United States of America* 99: 16660-5

Feng S, Xu Z, Peng J, Zhang M (2022) The AlkB Family: Potential Prognostic Biomarkers and Therapeutic Targets in Glioblastoma. *Frontiers in oncology* 12: 847821

Feng Y, Gao J, Yang M (2011) When MAGE meets RING: insights into biological functions of MAGE proteins. *Protein Cell* 2: 7-12

Fong KW, Zhao JC, Song B, Zheng B, Yu J (2018) TRIM28 protects TRIM24 from SPOP-mediated degradation and promotes prostate cancer progression. *Nature communications* 9: 5007

Fu D, Calvo JA, Samson LD (2012) Balancing repair and tolerance of DNA damage caused by alkylating agents. *Nat Rev Cancer* 12: 104-20

Ginn L, Maltas J, Baker MJ, Chaturvedi A, Wilson L, Guilbert R, Amaral FMR, Priest L, Mole H, Blackhall F et al. (2023) A TIAM1-TRIM28 complex mediates epigenetic silencing of protocadherins to promote migration of lung cancer cells. *Proceedings of the National Academy of Sciences of the United States of America* 120: e2300489120

788 Goodarzi AA, Kurka T, Jeggo PA (2011) KAP-1 phosphorylation regulates CHD3 nucleosome remodeling during the
789 DNA double-strand break response. *Nature structural & molecular biology* 18: 831-9
790 Gu J, Chen J, Xiang S, Zhou X, Li J (2023) Intricate confrontation: Research progress and application potential of
791 TRIM family proteins in tumor immune escape. *Journal of advanced research* 54: 147-179
792 Gu P, Deng W, Lei M, Chang S (2013) Single strand DNA binding proteins 1 and 2 protect newly replicated telomeres.
793 *Cell research* 23: 705-19
794 Han T, Tong W, Xie J, Guo X, Zhang L (2024) FOXF2 suppressed esophageal squamous cell carcinoma by reducing
795 M2 TAMs via modulating RNF144A-FTO axis. *International immunopharmacology* 143: 113422
796 Hatakeyama S (2011) TRIM proteins and cancer. *Nat Rev Cancer* 11: 792-804
797 Hegi ME, Diserens AC, Gorlia T, Hamou MF, de Tribolet N, Weller M, Kros JM, Hainfellner JA, Mason W, Mariani
798 L et al. (2005) MGMT gene silencing and benefit from temozolomide in glioblastoma. *The New England journal*
799 *of medicine* 352: 997-1003
800 Herquel B, Ouararhni K, Khetchoumian K, Ignat M, Teletin M, Mark M, Béchade G, Van Dorsselaer A, Sanglier-
801 Cianférani S, Hamiche A et al. (2011) Transcription cofactors TRIM24, TRIM28, and TRIM33 associate to form
802 regulatory complexes that suppress murine hepatocellular carcinoma. *Proceedings of the National Academy of*
803 *Sciences of the United States of America* 108: 8212-7
804 Ivanov AV, Peng H, Yurchenko V, Yap KL, Negorev DG, Schultz DC, Psulkowski E, Fredericks WJ, White DE, Maul
805 GG et al. (2007) PHD domain-mediated E3 ligase activity directs intramolecular sumoylation of an adjacent
806 bromodomain required for gene silencing. *Molecular cell* 28: 823-37
807 Jaiswal H, Benada J, Müllers E, Akopyan K, Burdova K, Koolmeister T, Helleday T, Medema RH, Macurek L,
808 Lindqvist A (2017) ATM/Wip1 activities at chromatin control Plk1 re-activation to determine G2 checkpoint
809 duration. *The EMBO journal* 36: 2161-2176
810 Jana S, Mondal M, Mahale S, Gupta B, Prasasvi KR, Kandasami L, Jha N, Chowdhury A, Santosh V, Kanduri C et al.
811 (2024) PITAR, a DNA damage-inducible cancer/testis long noncoding RNA, inactivates p53 by binding and
812 stabilizing TRIM28 mRNA. *eLife* 12
813 Jin X, Pan Y, Wang L, Zhang L, Ravichandran R, Potts PR, Jiang J, Wu H, Huang H (2017) MAGE-TRIM28 complex
814 promotes the Warburg effect and hepatocellular carcinoma progression by targeting FBP1 for degradation.
815 *Oncogenesis* 6: e312
816 Johannessen TC, Prestegarden L, Grudic A, Hegi ME, Tysnes BB, Bjerkvig R (2013) The DNA repair protein
817 ALKBH2 mediates temozolomide resistance in human glioblastoma cells. *Neuro Oncol* 15: 269-78
818 Ke B, Ye K, Cheng S (2020) ALKBH2 inhibition alleviates malignancy in colorectal cancer by regulating BMI1-
819 mediated activation of NF-κB pathway. *World journal of surgical oncology* 18: 328
820 Kim HJ, Lee JH, Kim SJ, Oh GS, Moon HD, Kwon KB, Park C, Park BH, Lee HK, Chung SY et al. (2010) Roles of
821 NADPH oxidases in cisplatin-induced reactive oxygen species generation and ototoxicity. *The Journal of*
822 *neuroscience : the official journal of the Society for Neuroscience* 30: 3933-46
823 Kim SH, Lee S, Lee CH, Lee MK, Kim YD, Shin DH, Choi KU, Kim JY, Park DY, Sol MY (2009) Expression of
824 cancer-testis antigens MAGE-A3/6 and NY-ESO-1 in non-small-cell lung carcinomas and their relationship with
825 immune cell infiltration. *Lung* 187: 401-11
826 Kuo CY, Li X, Kong XQ, Luo C, Chang CC, Chung Y, Shih HM, Li KK, Ann DK (2014) An arginine-rich motif of
827 ring finger protein 4 (RNF4) oversees the recruitment and degradation of the phosphorylated and SUMOylated
828 Krüppel-associated box domain-associated protein 1 (KAP1)/TRIM28 protein during genotoxic stress. *J Biol*

Chem 289: 20757-72

Le HP, Ma X, Vaquero J, Brinkmeyer M, Guo F, Heyer WD, Liu J (2020) DSS1 and ssDNA regulate oligomerization of BRCA2. *Nucleic acids research* 48: 7818-7833

Lee DH, Goodarzi AA, Adelmant GO, Pan Y, Jeggo PA, Marto JA, Chowdhury D (2012) Phosphoproteomic analysis reveals that PP4 dephosphorylates KAP-1 impacting the DNA damage response. *The EMBO journal* 31: 2403-15

Lee DH, Jin SG, Cai S, Chen Y, Pfeifer GP, O'Connor TR (2005) Repair of methylation damage in DNA and RNA by mammalian AlkB homologues. *J Biol Chem* 280: 39448-59

Leiros I, Nabong MP, Grøsvik K, Ringvoll J, Haugland GT, Uldal L, Reite K, Olsbu IK, Knaevelsrud I, Moe E et al. (2007) Structural basis for enzymatic excision of N1-methyladenine and N3-methylcytosine from DNA. *The EMBO journal* 26: 2206-17

Li J, Feng X, Liu Z, Deng Y, Sun Z, Chen B, Wu L, Wang X, Miao L, Zeng L et al. (2025) USP7 promotes temozolomide resistance by stabilizing MGMT in glioblastoma. *Cell death & disease* 16: 631

Li K, Krone MW, Butrin A, Bond MJ, Linhares BM, Crews CM (2024) Development of Ligands and Degraders Targeting MAGE-A3. *Journal of the American Chemical Society* 146: 24884-24891

Li Q, Huang Y, Liu X, Gan J, Chen H, Yang CG (2016) Rhein Inhibits AlkB Repair Enzymes and Sensitizes Cells to Methylated DNA Damage. *J Biol Chem* 291: 11083-93

Li X, Zeng H, Zhang L, Zhang J, Guo Y, Leng J (2024) An integrated LC-MS/MS platform for noninvasive urinary nucleus acid adductomics: A pilot study for tobacco exposure. *Journal of hazardous materials* 474: 134780

Li Y, Xie H, Liu S, Ruan Z, Wang B (2025) Resveratrol Alleviates Ischemia-Reperfusion-Induced Neuronal Damage by Inhibiting NR3C2-Mediated TRIM28 Expression. *Journal of integrative neuroscience* 24: 31375

Lin JR, Zeman MK, Chen JY, Yee MC, Cimprich KA (2011) SHPRH and HLTF act in a damage-specific manner to coordinate different forms of postreplication repair and prevent mutagenesis. *Molecular cell* 42: 237-49

Lin K, Zhou E, Shi T, Zhang S, Zhang J, Zheng Z, Pan Y, Gao W, Yu Y (2023) m6A eraser FTO impairs gemcitabine resistance in pancreatic cancer through influencing NEDD4 mRNA stability by regulating the PTEN/PI3K/AKT pathway. *J Exp Clin Cancer Res* 42: 217

Liu L, Xiao L, Liang X, Chen L, Cheng L, Zhang L, Wu X, Xu Q, Ma C (2017) TRIM28 knockdown increases sensitivity to etoposide by upregulating E2F1 in non-small cell lung cancer. *Oncology reports* 37: 3597-3605

Liu W, Zheng D, Huang X, Wei Z, Wei Z, Guo W (2025) TRIM17 promotes the progression of osteosarcoma by regulating PDK1 m6A modification-mediated AKT/mTOR pathway activation through ubiquitination of FTO. *Cell death & disease* 16: 767

Lombard DB, Kohler WJ, Guo AH, Gendron C, Han M, Ding W, Lyu Y, Ching TT, Wang FY, Chakraborty TS et al. (2020) High-throughput small molecule screening reveals Nrf2-dependent and -independent pathways of cellular stress resistance. *Science advances* 6

Lundholm L, Hååg P, Zong D, Juntti T, Mörk B, Lewensohn R, Viktorsson K (2013) Resistance to DNA-damaging treatment in non-small cell lung cancer tumor-initiating cells involves reduced DNA-PK/ATM activation and diminished cell cycle arrest. *Cell death & disease* 4: e478

Malacrida A, Di Domizio A, Bentivegna A, Cislaghi G, Messuti E, Tabano SM, Giussani C, Zuliani V, Rivara M, Nicolini G (2022) MV1035 Overcomes Temozolomide Resistance in Patient-Derived Glioblastoma Stem Cell Lines. *Biology* 11

Martin LP, Hamilton TC, Schilder RJ (2008) Platinum resistance: the role of DNA repair pathways. *Clinical cancer research : an official journal of the American Association for Cancer Research* 14: 1291-5

870 Meng S, Liu H, Xu J, Deng C, Qian X, Chu S, Zhu WG, Zhu J, Yong H, Li Z et al. (2025) PRMT5-Mediated ALKBH5
871 Methylation Promotes Colorectal Cancer Immune Evasion via Increasing CD276 Expression. *Research*
872 *(Washington, DC)* 8: 0549
873 Pineda CT, Potts PR (2015) Oncogenic MAGEA-TRIM28 ubiquitin ligase downregulates autophagy by ubiquitinating
874 and degrading AMPK in cancer. *Autophagy* 11: 844-6
875 Pineda CT, Ramanathan S, Fon Tacer K, Weon JL, Potts MB, Ou YH, White MA, Potts PR (2015) Degradation of
876 AMPK by a cancer-specific ubiquitin ligase. *Cell* 160: 715-728
877 Prince C, Hammerton G, Taylor AE, Anderson EL, Timpson NJ, Davey Smith G, Munafò MR, Relton CL, Richmond
878 RC (2019) Investigating the impact of cigarette smoking behaviours on DNA methylation patterns in adolescence.
879 *Hum Mol Genet* 28: 155-165
880 Randolph K, Hyder U, D'Orso I (2022) KAP1/TRIM28: Transcriptional Activator and/or Repressor of Viral and
881 Cellular Programs? *Frontiers in cellular and infection microbiology* 12: 834636
882 Ringvoll J, Nordstrand LM, Vågbø CB, Talstad V, Reite K, Aas PA, Lauritzen KH, Liabakk NB, Bjørk A, Doughty
883 RW et al. (2006) Repair deficient mice reveal mABH2 as the primary oxidative demethylase for repairing 1meA
884 and 3meC lesions in DNA. *The EMBO journal* 25: 2189-98
885 Saxena T, Quan A, Chan E, Kozlova N, Matai L, Lee JD, Rupaimoole R, Beca F, Muranen T, Slack FJ (2025) EGFR-
886 induced lncRNA TRIDENT promotes drug resistance in non-small cell lung cancer via phospho-TRIM28-
887 mediated DNA damage repair. *Proceedings of the National Academy of Sciences of the United States of America*
888 122: e2415389122
889 Soll JM, Sobol RW, Mosammaparast N (2017) Regulation of DNA Alkylation Damage Repair: Lessons and
890 Therapeutic Opportunities. *Trends in biochemical sciences* 42: 206-218
891 Song H, Feng X, Zhang H, Luo Y, Huang J, Lin M, Jin J, Ding X, Wu S, Huang H et al. (2019) METTL3 and ALKBH5
892 oppositely regulate m(6)A modification of TFEB mRNA, which dictates the fate of hypoxia/reoxygenation-treated
893 cardiomyocytes. *Autophagy* 15: 1419-1437
894 Song M, Yi F, Zeng F, Zheng L, Huang L, Sun X, Huang Q, Deng J, Wang H, Gu W (2024) USP18 Stabilized FTO
895 Protein to Activate Mitophagy in Ischemic Stroke Through Repressing m6A Modification of SIRT6. *Molecular*
896 *neurobiology* 61: 6658-6674
897 Tan Q, Ma J, Zhang H, Wu X, Li Q, Zuo X, Jiang Y, Liu H, Yan L (2022) miR-125b-5p upregulation by TRIM28
898 induces cisplatin resistance in non-small cell lung cancer through CREB1 inhibition. *BMC Pulm Med* 22: 469
899 Trewick SC, Henshaw TF, Hausinger RP, Lindahl T, Sedgwick B (2002) Oxidative demethylation by Escherichia coli
900 AlkB directly reverts DNA base damage. *Nature* 419: 174-8
901 Tsang YH, Wang Y, Kong K, Grzeskowiak C, Zagorodna O, Dogruluk T, Lu H, Villafane N, Bhavana VH, Moreno D
902 et al. (2020) Differential expression of MAGEA6 toggles autophagy to promote pancreatic cancer progression.
903 *eLife* 9
904 Tsao N, Brickner JR, Rodell R, Ganguly A, Wood M, Oyeniran C, Ahmad T, Sun H, Bacolla A, Zhang L et al. (2021)
905 Aberrant RNA methylation triggers recruitment of an alkylation repair complex. *Molecular cell* 81: 4228-4242.e8
906 Wada Y, Naito T, Fukushima T, Saito M (2024) Evaluation of ALKBH2 and ALKBH3 gene regulation in patients with
907 adult T-cell leukemia/lymphoma. *Virology journal* 21: 316
908 Wang C, Ivanov A, Chen L, Fredericks WJ, Seto E, Rauscher FJ, 3rd, Chen J (2005) MDM2 interaction with nuclear
909 corepressor KAP1 contributes to p53 inactivation. *The EMBO journal* 24: 3279-90
910 Wang K, Liu F, Muchu B, Deng J, Peng J, Xu Y, Li F, Ouyang M (2024) E3 ubiquitin ligase RNF180 mediates the

ALKBH5/SMARCA5 axis to promote colon inflammation and Th17/Treg imbalance in ulcerative colitis mice. *Archives of pharmacal research* 47: 645-658

Wang P, Wu J, Ma S, Zhang L, Yao J, Hoadley KA, Wilkerson MD, Perou CM, Guan KL, Ye D et al. (2015) Oncometabolite D-2-Hydroxyglutarate Inhibits ALKBH DNA Repair Enzymes and Sensitizes IDH Mutant Cells to Alkylating Agents. *Cell reports* 13: 2353-2361

Wang Z, Mierxiati A, Zhu W, Li T, Xu H, Wan F, Ye D (2025) FOXA1-dependent NSUN2 facilitates the advancement of prostate cancer by preserving TRIM28 mRNA stability in a m5C-dependent manner. *NPJ precision oncology* 9: 127

Wilson DL, Beharry AA, Srivastava A, O'Connor TR, Kool ET (2018) Fluorescence Probes for ALKBH2 Allow the Measurement of DNA Alkylation Repair and Drug Resistance Responses. *Angewandte Chemie (International ed in English)* 57: 12896-12900

Wu G, Yan Y, Cai Y, Peng B, Li J, Huang J, Xu Z, Zhou J (2021) ALKBH1-8 and FTO: Potential Therapeutic Targets and Prognostic Biomarkers in Lung Adenocarcinoma Pathogenesis. *Frontiers in cell and developmental biology* 9: 633927

Wu SS, Xu W, Liu S, Chen B, Wang XL, Wang Y, Liu SF, Wu JQ (2011) Down-regulation of ALKBH2 increases cisplatin sensitivity in H1299 lung cancer cells. *Acta pharmacologica Sinica* 32: 393-8

Xiao TZ, Suh Y, Longley BJ (2014) MAGE proteins regulate KRAB zinc finger transcription factors and KAP1 E3 ligase activity. *Archives of biochemistry and biophysics* 563: 136-44

Xu GL, Bochtler M (2020) Reversal of nucleobase methylation by dioxygenases. *Nature chemical biology* 16: 1160-1169

Xu L, Zhang K, Ma X, Li Y, Jin Y, Liang C, Wang Y, Duan W, Zhang H, Zhang Z et al. (2022) Boosting cisplatin chemotherapy by nanomotor-enhanced tumor penetration and DNA adducts formation. *Journal of nanobiotechnology* 20: 429

Yalçin Z, Lam SY, Peuscher MH, van der Torre J, Zhu S, Iyengar PV, Salas-Lloret D, de Krijger I, Moatti N, van der Lugt R et al. (2024) UBE2D3 facilitates NHEJ by orchestrating ATM signalling through multi-level control of RNF168. *Nature communications* 15: 5032

Yang CG, Yi C, Duguid EM, Sullivan CT, Jian X, Rice PA, He C (2008) Crystal structures of DNA/RNA repair enzymes AlkB and ABH2 bound to dsDNA. *Nature* 452: 961-5

Yi C, He C (2013) DNA repair by reversal of DNA damage. *Cold Spring Harbor perspectives in biology* 5: a012575

Zhang L, Liu M, Xie Y, Yuan BF, Peng Z, Xiong J, Zhang XL (2025) FTO O-GlcNAcylation promotes TRIM21-mediated FTO ubiquitination degradation to sustain the negative feedback control of macrophage inflammation. *Front Immunol* 16: 1593243

Zhao W, Zheng HZ, Zhou T, Hong XS, Cui HJ, Jiang ZW, Chen HJ, Zhou ZJ, Liu XG (2017) CTT1 overexpression increases the replicative lifespan of MMS-sensitive Saccharomyces cerevisiae deficient in KSP1. *Mechanisms of ageing and development* 164: 27-36

Zhao Y, Majid MC, Soll JM, Brickner JR, Dango S, Mosammaparast N (2015) Noncanonical regulation of alkylation damage resistance by the OTUD4 deubiquitinase. *The EMBO journal* 34: 1687-703

Zhou X, Xia Q, Wang B, Li J, Liu B, Wang S, Huang M, Zhong R, Cheng SY, Wang X et al. (2025) USP14 modulates stem-like properties, tumorigenicity, and radiotherapy resistance in glioblastoma stem cells through stabilization of MST4-phosphorylated ALKBH5. *Theranostics* 15: 2293-2314

952 **Figure legends**

953 **Figure 1. TRIM28 directly binds ALKBH2. (A)** Silver staining and LC–MS/MS identification
954 of ALKBH2 as a TRIM28-associated protein following affinity purification in H1299 NSCLC
955 cells. The TRIM28 band is indicated. **(B)** Co-immunoprecipitation (co-IP) analysis of HEK293T
956 cells co-expressing HA-ALKBH2 and Flag-TRIM28 or Flag-TRIM24. Anti-Flag
957 immunoprecipitates were analyzed by western blotting (WB). **(C)** Reciprocal co-IP using HA-
958 ALKBH2 and Flag-TRIM28 (or HA-GFP control) with anti-HA immunoprecipitation. **(D)**
959 Schematic of full-length TRIM28 and truncation mutants. **(E)** Domain mapping using Flag-IP in
960 HEK293T cells co-transfected with HA-ALKBH2 and Flag-TRIM28 truncation mutants. **(F)**
961 Endogenous ALKBH2–TRIM28 interaction in H1299 cells detected by co-IP with anti-TRIM28
962 antibody. **(G)** Immunofluorescence (IF) showing nuclear co-localization of endogenous ALKBH2
963 (green) and TRIM28 (red). Nuclei were counterstained with DAPI (blue). Scale bar, 20 μm.
964 Pearson correlation coefficient (PCC) = 0.896 ± 0.016 (mean ± SD, n = 42). **(H)** *In vitro* MBP
965 pull-down assay using recombinant His-Flag-ALKBH2 and purified MBP-TRIM28. **(I)**
966 Specificity profiling of endogenous TRIM28 binding in HEK293T cells transfected with Flag-
967 ALKBH2 or Flag-ALKBH3. **(J)** GRAMM-X docking of TRIM28 RBCC (cyan) with ALKBH2
968 (light red) or ALKBH3 (green). Middle: Magnified interface showing ALKBH2 Finger and Long-
969 loop motifs (red). Right: Superposition with ALKBH2–DNA (orange), revealing overlap of
970 TRIM28- and DNA-binding surfaces. **(K)** Flag-IP analysis of lysates from Flag-ALKBH2-
971 expressing HEK293T cells in the presence of increasing ssDNA concentrations. Data are
972 representative of n ≥ 3 biological replicates.

973

974 **Figure 2. TRIM28 promotes K48-linked ubiquitination and proteasomal degradation of**
975 **ALKBH2. (A)** *In vivo* ubiquitination assay in HEK293T cells co-transfected with Flag-ALKBH2
976 and HA-ubiquitin (Ub), treated with MG132 (10 μM, 6 h). Lysates were subjected to denaturing
977 IP (1% SDS) with anti-Flag antibody. **(B)** Denaturing Flag-IP analysis of HEK293T cells co-
978 transfected with Flag-ALKBH2 and HA-tagged wild-type (WT), K48-only, or K48R ubiquitin
979 mutants. **(C)** K48-linked polyubiquitin enrichment using Halo-TUBE beads from HEK293T cells

980 expressing Flag-ALKBH2 treated with MG132. **(D)** Denaturing Flag-IP of HEK293T cells co-
981 transfected with Flag-ALKBH2, His-TRIM28, and HA-K48-only ubiquitin. **(E)** Analysis of
982 ALKBH2 ubiquitination in HEK293T cells co-transfected with Flag-ALKBH2 and WT or RING-
983 inactive (C65/68A) His-TRIM28. **(F)** Denaturing Flag-IP detecting K48-linked ALKBH2
984 ubiquitination in TRIM28-knockdown HEK293T cells reconstituted with shRNA-resistant
985 TRIM28 (WT). **(G)** WB analysis of H1299 and A549 cells transduced with control (shCon) or
986 TRIM28-specific shRNAs. **(H)** qRT-PCR quantification of ALKBH2 mRNA in H1299 cells
987 following TRIM28 depletion. **(I)** WB analysis of ALKBH2 levels in H1299 and HEK293T cells
988 overexpressing increasing doses of TRIM28. **(J)** WB analysis of H1299 cells transduced with
989 control or ALKBH2-specific shRNAs. **(K)** WB analysis of ALKBH2-depleted cells reconstituted
990 with Flag-ALKBH2. **(L)** qRT-PCR of TRIM28 transcript levels in H1299 cells expressing empty
991 vector or Flag-ALKBH2. Data are representative of $n \geq 3$ biological replicates. Error bars indicate
992 mean ± SD. $*p < 0.05$, $**p < 0.01$ (unpaired, two-tailed Student's t-test). NS, not significant.
993

994 **Figure 3. MAGEA6 scaffolds the TRIM28–ALKBH2 E3 ligase complex and promotes**
995 **ALKBH2 degradation. (A)** Anti-Flag IP analysis of the interaction between Myc-MAGEA6 and
996 Flag-ALKBH2 (or GFP control) in HEK293T cells. **(B)** *In vitro* pulldown assay using recombinant
997 His-Flag-ALKBH2 and purified MBP-MAGEA6. **(C)** Anti-Flag IP in HEK293T cells (± TRIM28
998 knockdown) co-transfected with HA-ALKBH2 and Flag-MAGEA6. **(D)** Flag-IP analysis of the
999 ALKBH2–TRIM28 interaction in HEK293T cells transfected with Myc-MAGEA6. **(E)** HA-IP in
1000 H1299 cells stably expressing HA-ALKBH2 following MAGEA3/6 knockdown. **(F)** K48-specific
1001 Halo-TUBE pulldown in TRIM28-knockdown HEK293T cells overexpressing Myc-MAGEA6.
1002 **(G)** WB analysis of ALKBH2 stability in control or TRIM28-knockout (sgTRIM28) H1299 cells
1003 transfected with MAGEA6 and treated with cycloheximide (CHX, 150 μg/mL). **(H)** Flag-IP
1004 mapping of interactions between Flag-MAGEA6 (WT or mutants), endogenous TRIM28, and co-
1005 expressed HA-ALKBH2 in HEK293T cells. **(I)** K48-specific Halo-TUBE pulldown of
1006 ubiquitinated proteins in HEK293T cells co-expressing HA-ALKBH2 and Flag-MAGEA6 (WT

1007 or mutants). **(J)** Anti-Flag IP of HEK293T cells transfected with HA-ALKBH2 and cancer-
1008 associated Flag-MAGEA6 mutants. Data are representative of n ≥ 3 biological replicates.
1009
1010 **Figure 4. MMS dynamically regulates the TRIM28–ALKBH2 pathway. (A)** Anti-Flag IP from
1011 H1299 cells expressing HA-ALKBH2 and Flag-TRIM28 treated with MMS (100 μM) and MG132
1012 (10 μM) for the indicated times. **(B)** Anti-Flag IP from H1299 cells expressing Flag-TRIM28
1013 treated with indicated MMS concentrations (3 h, +MG132). **(C)** WB analysis of MAGEA3/6 in
1014 nuclear/cytoplasmic fractions of H1299 cells treated with MMS (100 μM, 4 h). **(D)** Denaturing
1015 anti-Flag IP of H1299 cells expressing Flag-ALKBH2 treated with MMS (0–200 μM, 3 h) plus
1016 MG132. **(E)** Degradation assay in H1299 cells expressing TAP-ALKBH2 transduced with Flag-
1017 TRIM28 or vector, treated with MMS (100 μM). **(F)** Anti-Flag IP of cell lysates incubated with
1018 ssDNA (1 μM), H_2O_2 (200 μM), Vc (500 μM), or EDTA (5 mM). **(G)** Anti-Flag IP assessing the
1019 effect of EDTA (5 mM) on H_2O_2-induced interactions in ssDNA-containing lysates. **(H)** K48-
1020 specific Halo-TUBE pulldown in H1299 cells expressing TAP-ALKBH2 treated with MG132 (10
1021 μM), MMS (100 μM), and Vc (500 μM) for 8 h. **(I)** WB of ALKBH2 in H1299 and H460 cells
1022 treated with MMS (100 μM). **(J)** Quantification of ALKBH2 protein levels from (I). **(K)** WB
1023 analysis of H1299 cells expressing HA-TRIM28 treated with MMS (100 μM). **(L)** qRT-PCR of
1024 ALKBH2 in H1299 cells treated with MMS (100 μM). Data are representative of n ≥ 3 biological
1025 replicates. Error bars indicate mean ± SD. *$p < 0.05$, **$p < 0.01$ (unpaired, two-tailed Student's t-
1026 test).
1027
1028 **Figure 5. MMS induces K48-linked ubiquitination and proteasomal degradation of TRIM28.**
1029 **(A, B)** WB analysis of TRIM28 levels in H1299 cells treated with MMS in a time- (A) and dose-
1030 dependent (B) manner. **(C)** qRT-PCR of TRIM28 mRNA in cells treated with MMS (100 μM). **(D)**
1031 Denaturing anti-Flag IP of HEK293T cells expressing Flag-TRIM28 and HA-Ub treated with
1032 MMS and MG132. **(E)** Anti-Flag IP and K48-specific Ub WB in H1299 cells expressing Flag-
1033 TRIM28 treated with MMS (100 μM) + MG132. **(F)** Denaturing anti-Flag IP in HEK293T cells

1034 transfected with Flag-TRIM28 and HA-Ub (K48-only) treated with MMS (100 μM). **(G)** K48-
1035 specific Halo-TUBE pulldown of endogenous TRIM28 in H1299 cells treated with MG132 and
1036 increasing MMS. **(H)** Halo-TUBE pulldown comparing effects of MMS (200 μM), temozolomide
1037 (TMZ, 200 μM), cisplatin (CDDP, 20 μM), or H_2O_2 (300 μM) on TRIM28 ubiquitination
1038 (+MG132, 6 h). **(I)** Halo-TUBE pulldown in HEK293T cells expressing Flag-TRIM28 WT or
1039 SUMO-deficient mutant (K554/779/804R) treated with MMS. **(J)** Anti-Flag co-IP in H1299 cells
1040 expressing Flag-TRIM28 treated with MMS (100 μM) + MG132. **(K)** Anti-Flag co-IP in
1041 HEK293T cells expressing Flag-TRIM28 and Myc-MAGEA6 treated with MMS. **(L)** Anti-Flag
1042 co-IP and WB in HEK293T cells expressing Flag-TRIM24 treated with MMS + MG132. (M)
1043 Halo-TUBE enrichment of K48-linked proteins in HEK293T cells overexpressing Flag-TRIM24
1044 treated with MMS. Data are representative of n ≥ 3 biological replicates. Error bars indicate mean
1045 ± SD. NS, not significant.
1046
1047 **Figure 6. The TRIM28–ALKBH2 axis is clinically relevant and regulates sensitivity to**
1048 **alkylation damage. (A)** Relative mRNA expression of ALKBH2, ALKBH3, and MGMT in
1049 LUAD vs. normal lung (TCGA dataset; Mann–Whitney test). **(B)** Representative ALKBH2
1050 immunohistochemistry (IHC) staining in LUAD and matched normal lung (Human Protein Atlas).
1051 **(C)** WB analysis of ALKBH2, TRIM28, ALKBH3, and MGMT in NSCLC cell lines and BEAS-
1052 2B cells. **(D, E)** Kaplan–Meier overall survival for LUAD patients stratified by ALKBH2 (D) or
1053 ALKBH3 (E) mRNA expression. **(F)** CCK-8 proliferation assay in H1299 cells following
1054 ALKBH2 knockdown. **(G)** CCK-8 viability assay in H1299 cells (ALKBH2 knockdown) 48 h
1055 after a 1 h MMS pulse. **(H)** CCK-8 viability assay in H1299 cells overexpressing Flag-TRIM28
1056 WT or RING-inactive mutant (C65/68A) after MMS pulse. **(I)** MMS sensitivity assessment in
1057 H1299 cells with TRIM28 knockdown and rescue. **(J)** Rescue of MMS hypersensitivity in H1299
1058 cells by ALKBH2 co-expression. **(K)** Effect of MAGEA6 overexpression on MMS cytotoxicity.
1059 **(L)** Effect of TRIM28-binding-deficient MAGEA6 mutant (D156E/S157Y) on MMS sensitivity.
1060 Data are representative of n ≥ 3 biological replicates. Error bars indicate mean ± SD. *$p < 0.05$,

1061 **$p < 0.01$ (unpaired, two-tailed Student's t-test).

1062

1063 **Figure 7. Combining MMS with CDDP synergistically enhances cancer cell killing. (A)** CCK-
1064 8 viability assay of H1299 cells (TRIM28 knockdown) treated with continuous low-dose MMS
1065 (48 h). **(B, C)** Colony formation assay of H460 cells overexpressing TRIM28 treated with MMS
1066 (100 μM, 48 h). Representative images (B) and quantification (C). **(D)** CCK-8 assay of H1299
1067 cells (ALKBH2 knockdown rescued with Flag-ALKBH2) treated with MMS ± 2 μM CDDP. **(E)**
1068 Alkaline comet assay of H1299 cells treated with MMS (50 μM) and/or CDDP (2 μM). Tail
1069 moments quantified (n = 70). **(F, G)** IC_{50} analysis of CDDP in H1299 (F) and H460 (G) cells with
1070 MMS co-treatment. **(H, I)** Clonogenic survival of H460 cells treated with MMS (75 μM) and
1071 CDDP (1 μM). **(J, K)** 3D tumor spheroid growth of H1299 cells treated with MMS (100 μM) and
1072 CDDP (2 μM). Calcein-AM (live cells)/PI (dead cells) staining (J) and volume quantification (K).
1073 Scale bar: 200 μm. Data are representative of n ≥ 3 biological replicates. Error bars indicate mean
1074 ± SD. *$p < 0.05$, **$p < 0.01$ (unpaired, two-tailed Student's t-test).

1075

1076 **Figure 8. Model of the biphasic TRIM28–ALKBH2 regulatory switch induced by alkylation**
1077 **stress. (I) Basal state.** MAGEA6-assisted, TRIM28-mediated K48-linked ubiquitination
1078 maintains low ALKBH2 levels; ALKBH2 supports TRIM28 transcription. **(II) Acute MMS:**
1079 Enhanced assembly of the TRIM28–MAGEA6–ALKBH2 complex accelerates ALKBH2
1080 degradation. **(III) Prolonged MMS:** Ubiquitin flux shifts toward TRIM28, leading to its
1081 degradation and releasing ubiquitin-dependent repression of ALKBH2, together with MMS-
1082 induced transcriptional activation that drives progressive ALKBH2 accumulation.

1083 **Expanded view figure legends**

1084 **Figure EV1. MAGEA6 supports TRIM28-dependent ubiquitination of ALKBH2 (Related to**
1085 **Fig. 3). (A)** HA-IP in HEK293T cells transfected with HA-ALKBH2, Flag-TRIM28, and
1086 increasing Myc-MAGEA6. **(B)** Anti-Flag IP in HEK293T cells co-transfected with HA-ALKBH2,
1087 Flag-TRIM28, and Myc-MAGEA6 or Myc-MAGEC2. **(C)** Halo-TUBE enrichment of K48-
1088 ubiquitinated proteins in H1299 cells (MAGEA6 knockdown) reconstituted with Flag-MAGEA6.
1089 **(D)** Sequence alignment of MAGEA6 WT and MutA/MutB variants. **(E)** WB analysis of ALKBH2
1090 stability in H1299 cells expressing WT or mutant MAGEA6 treated with CHX. **(F)** AlphaFold3
1091 structural model of the MAGEA6–TRIM28 complex. **(G)** ALKBH2 degradation assay in H1299
1092 cells expressing WT or TRIM28-binding-deficient (D156E/S157Y) MAGEA6 treated with CHX.
1093 **(H)** Anti-Flag IP of HEK293T cells transfected with WT or mutant Flag-MAGEA6. Data are
1094 representative of n ≥ 3 biological replicates.

1095

1096 **Figure EV2. Redox-modulated regulation of the TRIM28–ALKBH2 pathway under MMS**
1097 **exposure (Related to Fig. 4). (A)** IF staining of Flag-ALKBH2 (red) and TRIM28 (green) in
1098 H1299 cells treated with MMS (100 μM, 8 h). Nuclei stained with DAPI. Scale bar = 20 μm. **(B)**
1099 WB analysis of ALKBH2 turnover in H1299 cells treated with CHX, MMS, or both. **(C)**
1100 Quantification of ALKBH2 levels from (B). **(D)** Anti-Flag IP of lysates in the presence of GSSG
1101 (1 mM), GSH (1 mM), or H_2O_2 (0.5 mM). **(E)** Anti-Flag IP in H1299 cells expressing Flag-
1102 ALKBH2 treated with H_2O_2 + MG132. **(F)** Anti-Flag IP of WT or mutant ALKBH2
1103 (H171A/D173A) in the presence of ssDNA or H_2O_2. Data are representative of n ≥ 3 biological
1104 replicates. Error bars indicate mean ± SD. $*p < 0.05$, $**p < 0.01$.

1105

1106 **Figure EV3. Extended analyses of MMS-induced ubiquitination and degradation of TRIM28**
1107 **(Related to Fig. 5). (A)** WB of H1299 cells treated with MMS (100 μM) for indicated durations.
1108 **(B)** WB monitoring ALKBH2 turnover (CHX chase) in H1299 cells pretreated with MMS (100
1109 μM, 12 h). **(C)** Quantification of ALKBH2 levels from (B). **(D)** WB of H1299 cells treated with

1110 TMZ (100 μM). **(E, F)** WB analysis of H1299 cells treated with CDDP (E) or H_2O_2 (F). **(G)** WB
1111 analysis of anti-Flag immunoprecipitates and whole-cell lysates from H1299 cells expressing WT
1112 or mutant Flag-TRIM28 treated with MMS. **(H)** WB of TRIM28 levels in HEK293T cells
1113 overexpressing Flag-TRIM24 treated with MMS. **(I)** Quantification of TRIM28 levels from (H).
1114 Data are representative of n ≥ 3 biological replicates. Error bars indicate mean ± SD. *$p < 0.05$,
1115 **$p < 0.01$.
1116

1117 **Figure EV4. Clinical and functional analyses supporting the TRIM28–ALKBH2 axis in**
1118 **NSCLC (Related to Fig. 6). (A)** CPTAC analysis (UALCAN) of ALKBH2, ALKBH3, and
1119 MGMT protein expression in LUAD vs. normal lung. **(B)** ALKBH2 mRNA expression in LUAD
1120 patients by smoking history (UALCAN/TCGA). **(C)** Frequency of MAGEA6 and MAGEA3
1121 mutations in TCGA lung cancer samples stratified by smoking status (Fisher's exact test). **(D)** WB
1122 of TRIM28 in H1299 cells after short-term high-dose MMS (500 μM, 1 h) and release. **(E)** CCK-
1123 8 proliferation assay of H1299 cells overexpressing TRIM28. **(F)** CCK-8 survival assay in
1124 MAGEA6-knockdown H1299 cells with MAGEA6 re-expression. **(G, H)** CCK-8 viability assay
1125 of H1299 cells expressing Flag-MAGEA6 treated with CDDP (G) or bortezomib (BTZ) (H). Data
1126 are representative of n ≥ 3 biological replicates. Error bars indicate mean ± SD. *$p < 0.05$, **$p <$
1127 0.01.
1128

1129 **Figure EV5. Additional analyses supporting the combined effects of MMS and CDDP on**
1130 **cytotoxicity (Related to Fig. 7). (A)** Summary of therapeutic agents for lung cancer patients
1131 (TCGA–GDC database). **(B, C)** Kaplan–Meier survival analysis of patients who received
1132 chemotherapy (B) versus those who did not receive chemotherapy (C), stratified by high vs. low
1133 TRIM28 mRNA levels. **(D)** CCK-8 viability assay of H1299 cells treated with low-dose MMS ±
1134 H_2O_2. **(E)** WB of γ-H2AX in H1299 cells treated with CDDP ± MMS. **(F)** IC_{50} determination of
1135 MMS in H1299 and H460 cells (CCK-8). Data are representative of n ≥ 3 biological replicates.
1136 Error bars indicate mean ± SD. *$p < 0.05$, **$p < 0.01$.

Figure 1 (Sun et al.)

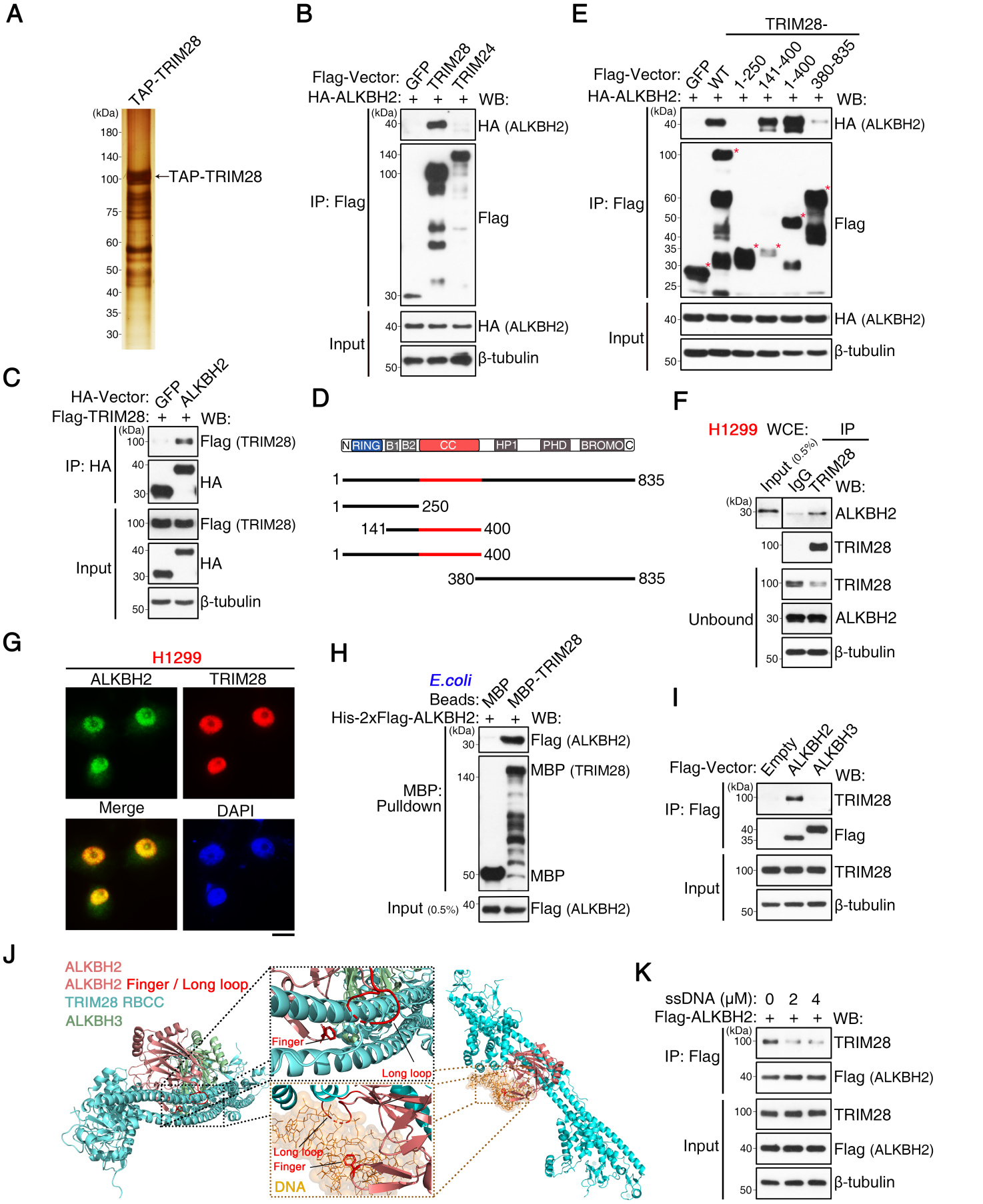

Figure 2 (Sun et al.)

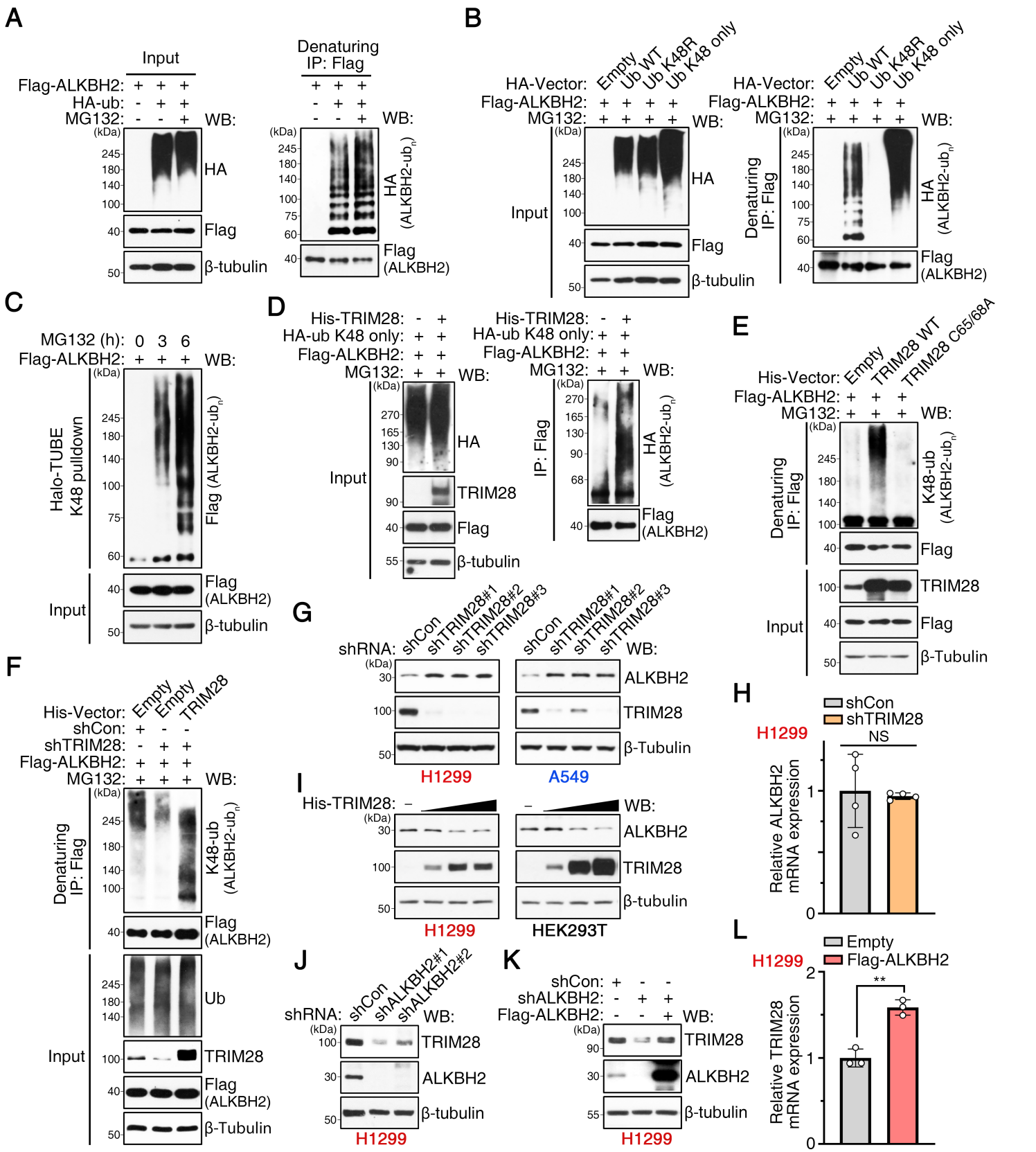

Figure 3 (Sun et al.)

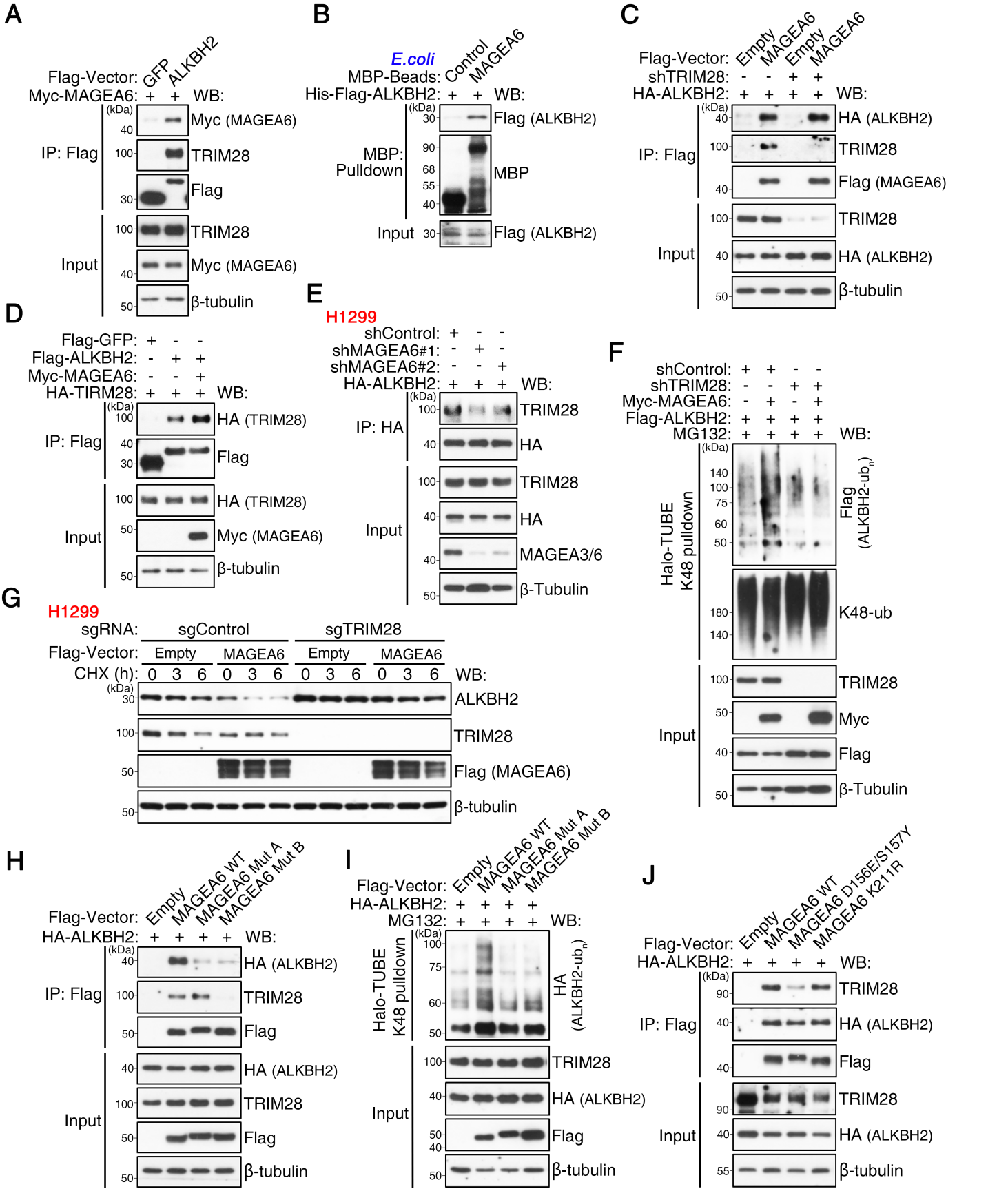

Figure 4 (Sun et al.)

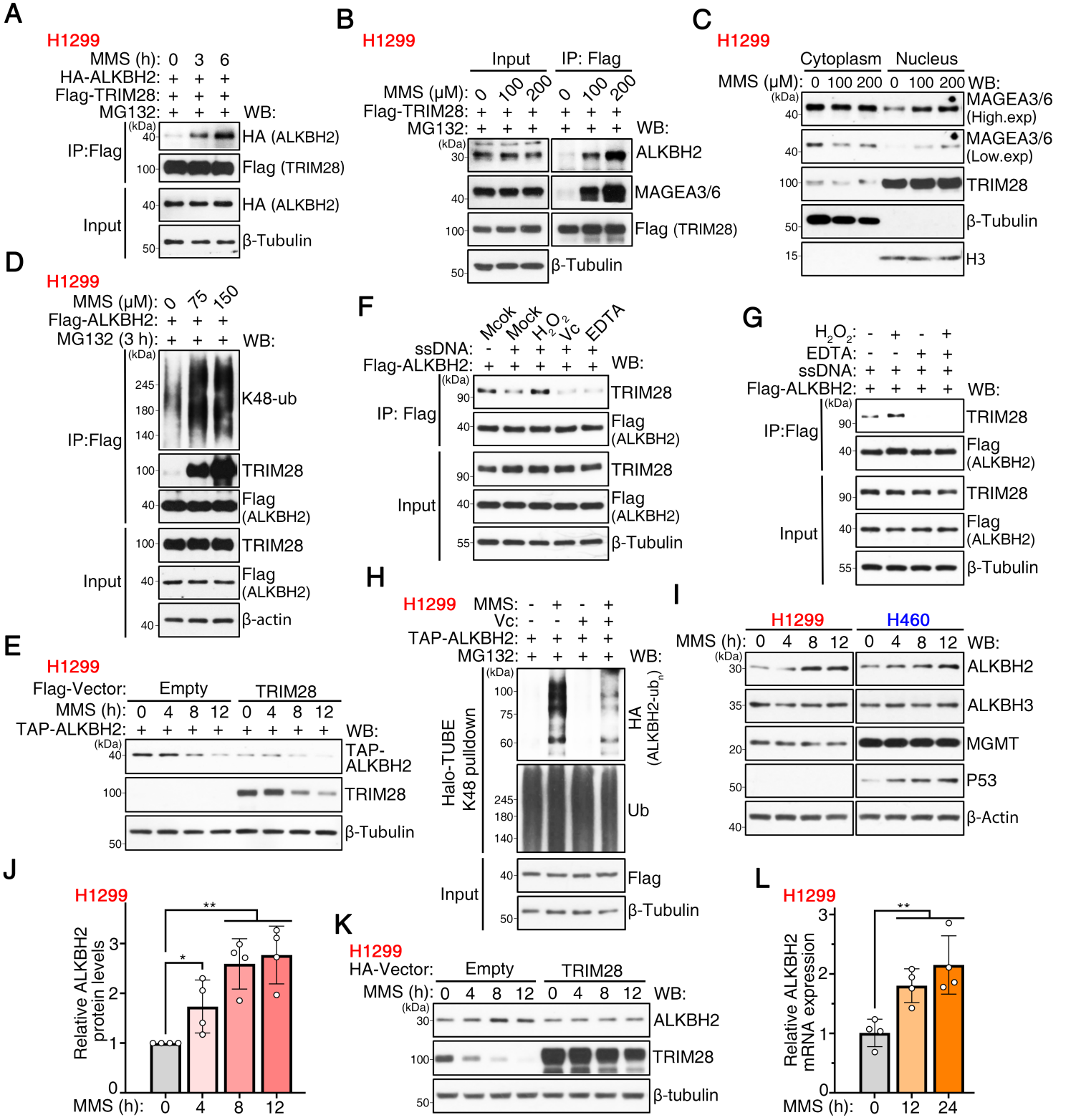

Figure 5 (Sun et al.)

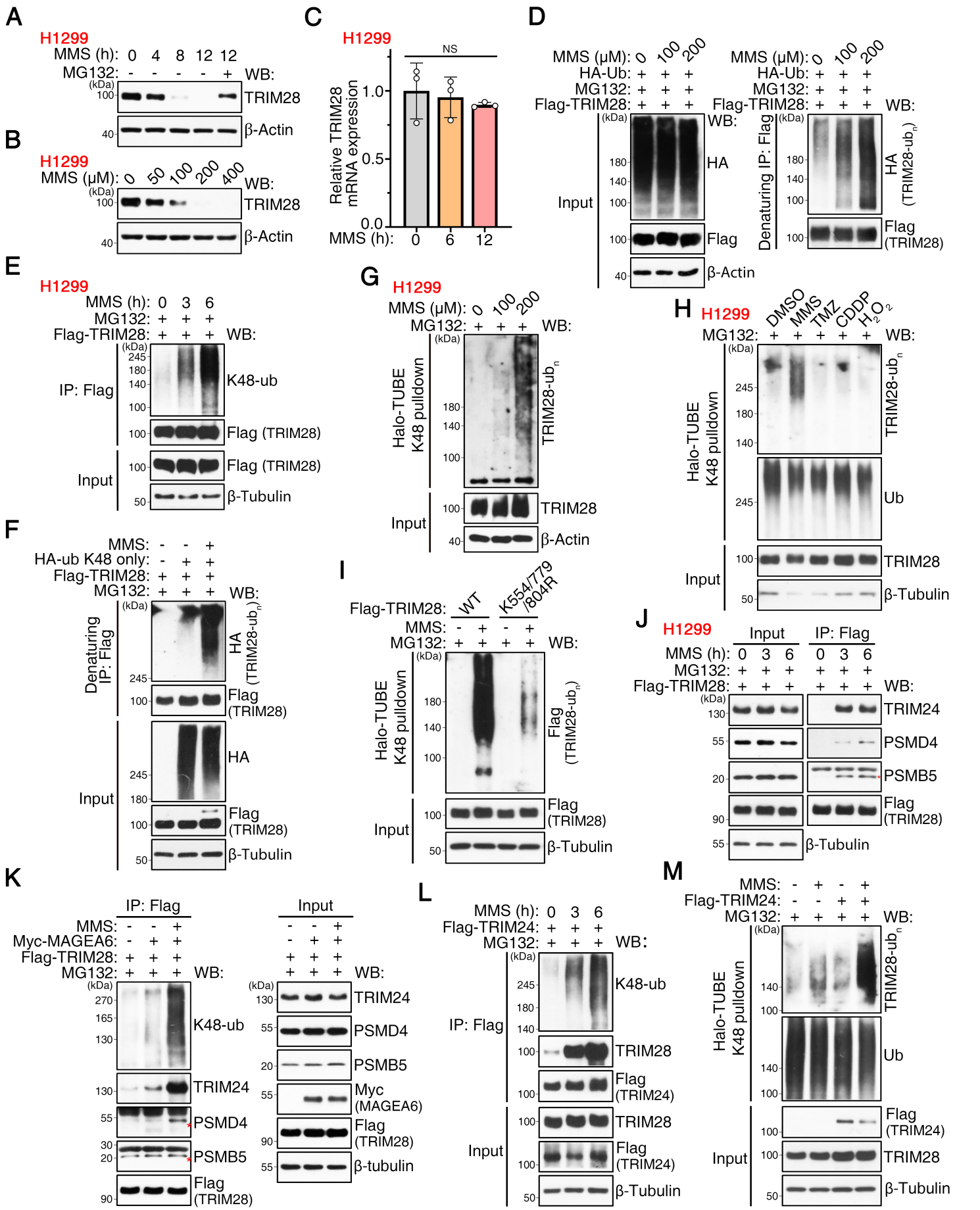

Figure 6 (Sun et al.)

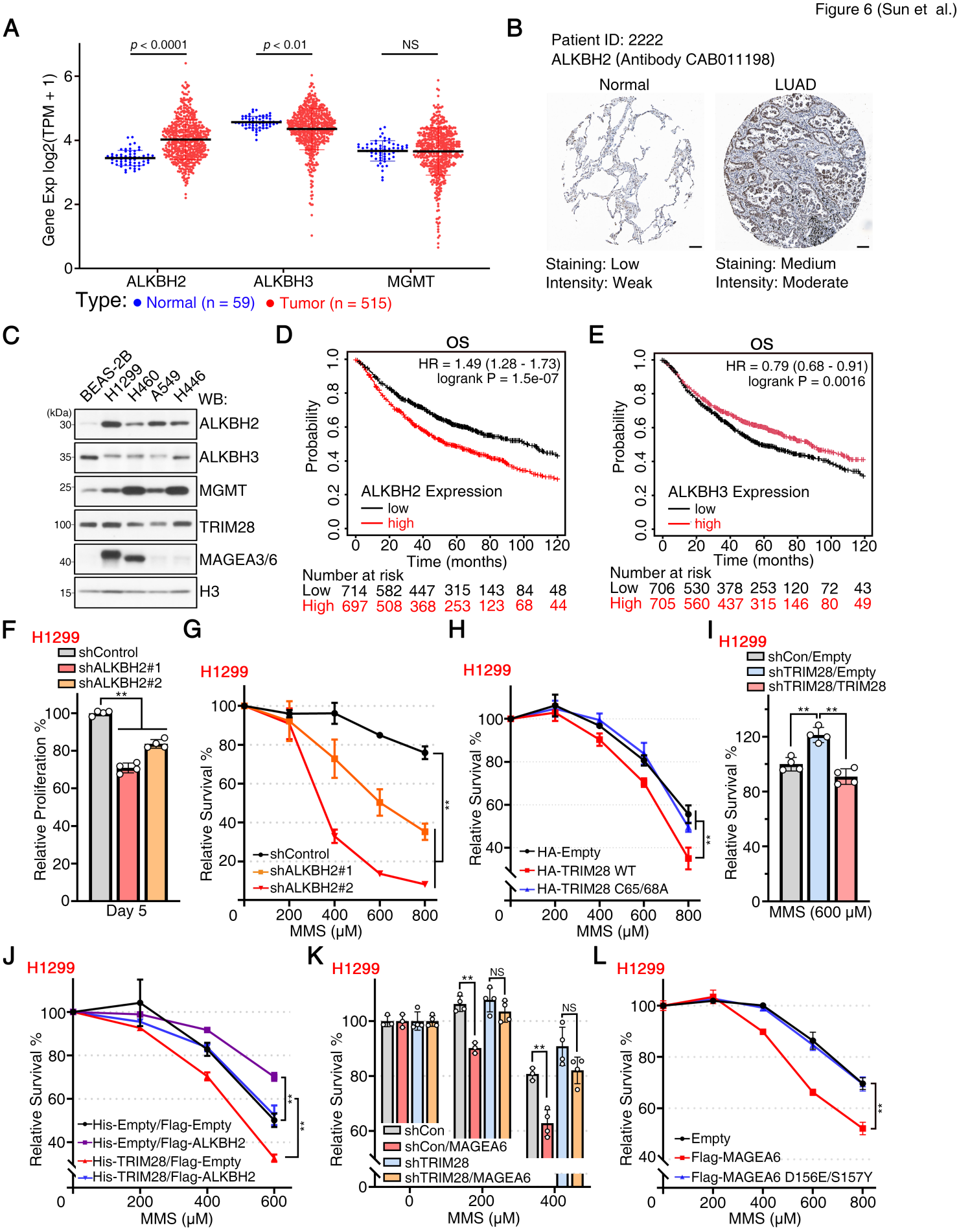

Figure 7 (Sun et al.)

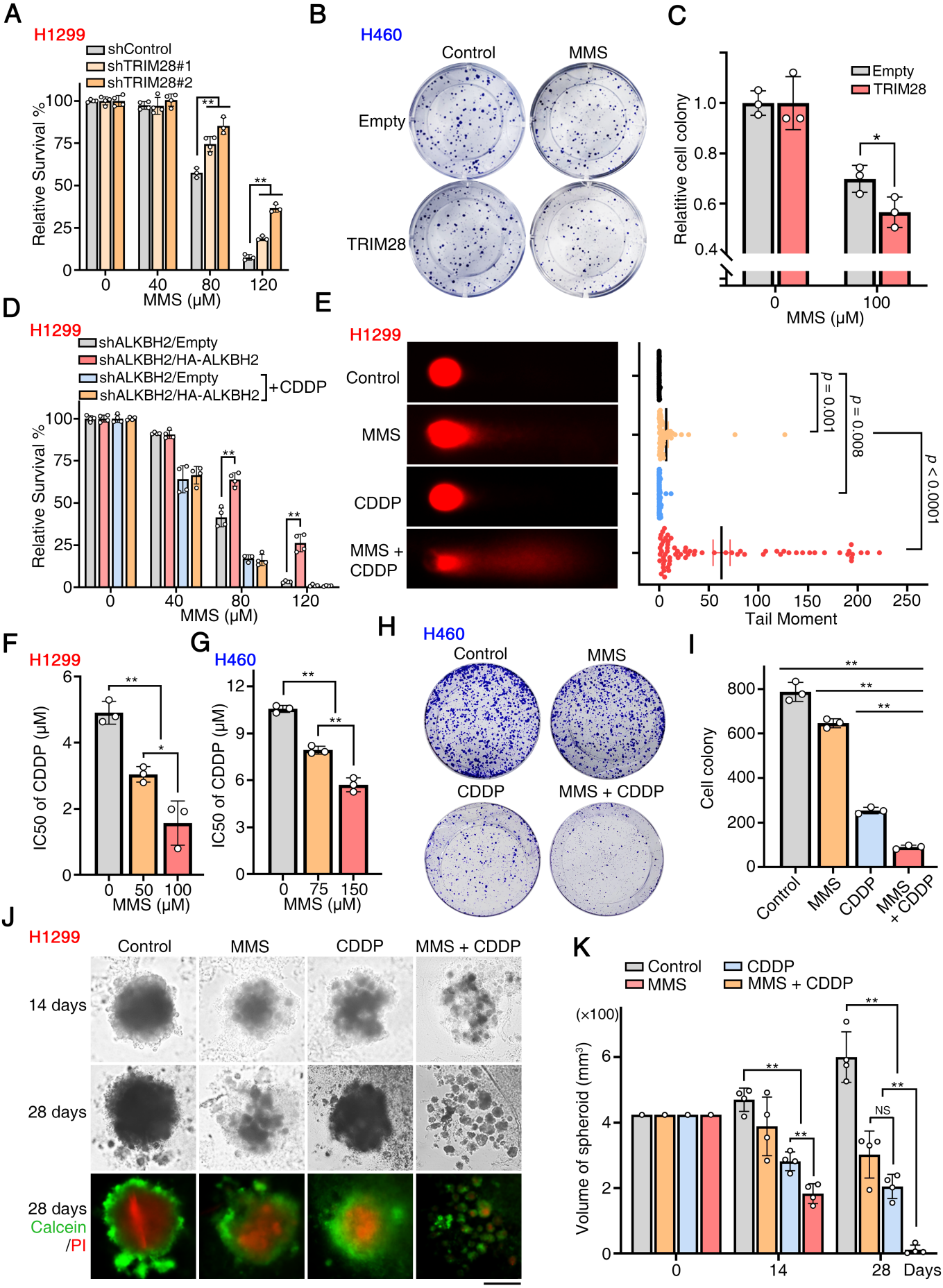
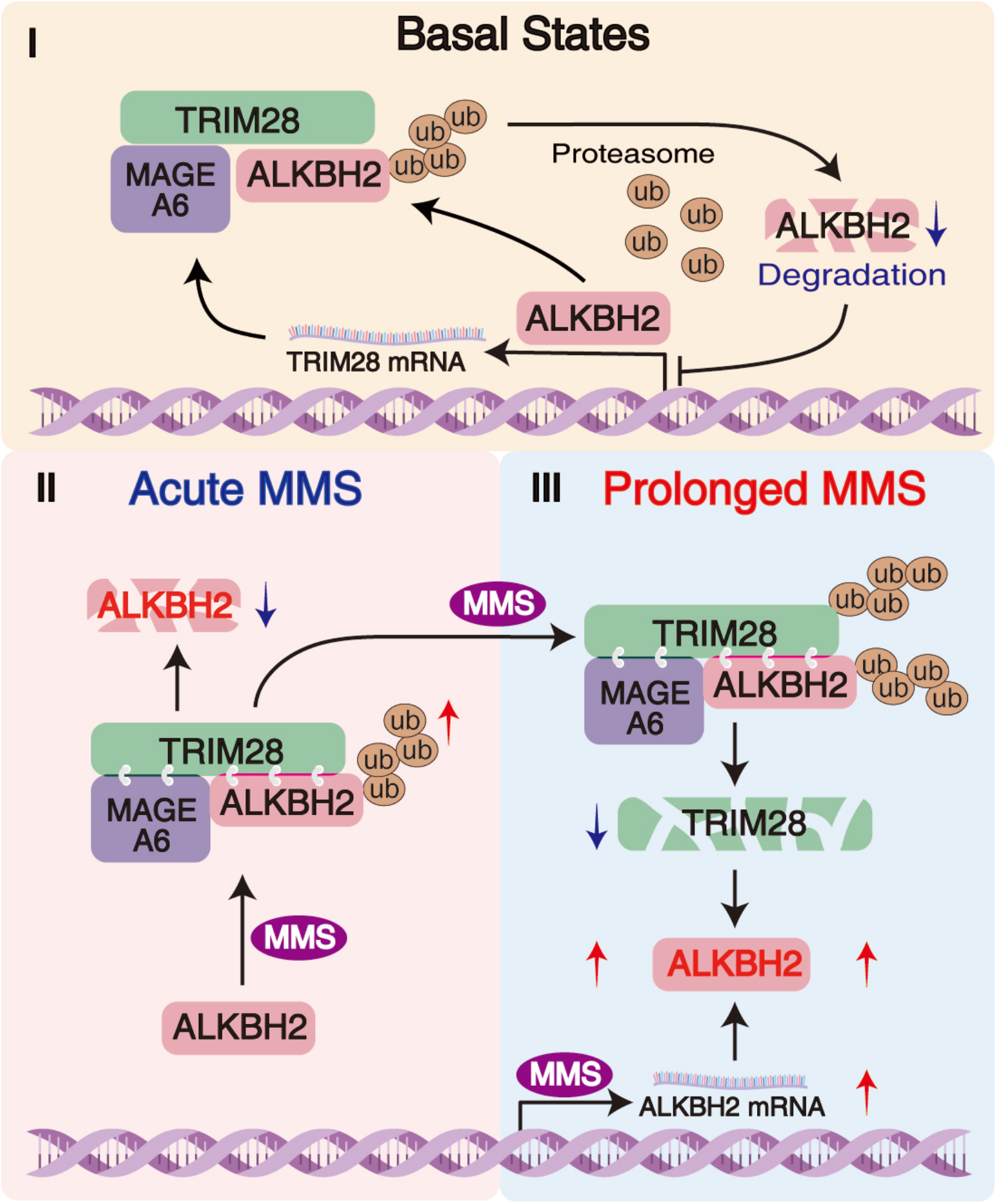
Figure 8 (Sun et al.)